The CMS Micro-strip Gas Chamber project – Development of a high resolution tracking detector for harsh radiation environments

R. Bellazzini [a,c] M. Bozzo [b,c] A. Brez [a] A. Cattai [c] G. Gariano [a]
L. Latronico [b] R. Loni [a] N. Lumb [a] A. Moggi [a] A. Morelli [a]
A. Papanestis [a] S. Reale [a] C. Salaris [a] G. Spandre [a]
M.M. Massai [a] M.A. Spezziga [a] A. Toropin [a,d]

[a] *INFN-Pisa and University of Pisa, Pisa, Italy*
[b] *INFN-Genova and University of Genova, Genova, Italy*
[c] *CERN, CH-1211 Geneva 23, Switzerland*
[d] *INR, Russian Academy of Sciences, Moscow, Russia*

Thirty-two large area Micro-Strip Gas Chambers were tested in a high intensity, 350 MeV pion beam at PSI to prove that we had reached a Milestone for the Compact Muon Solenoid (CMS) experiment. The particle rate was approximately 6 kHz/mm^2, distributed over the whole active area of the detectors, and this rate was maintained for a total integrated time of 493 hours. All of the chambers were operated with signal-to-noise values at or above that corresponding to 98 % hit detection efficiency at CMS; the average S/N was 31. No indications of any gain instabilities or ageing effects were observed. In the official 3-week Milestone period, three strips from a total of 16384 were damaged, a result which is twenty times lower than the minimal requirement for CMS. The spark rate of the detectors was very low and decreased with time to an average of one spark per chamber per day. The cathode voltages of 24 of the chambers were increased over a one week period to investigate the behaviour of the detectors at higher gains; the maximum S/N value was 2.4 times that at the normal working point. No significant increase in spark rate or strip loss rate was detected and the chambers operated stably. The detector efficiencies and imaging capabilities were also investigated. The MSGC design features and the assembly and test methodologies that enabled us to achieve these results are reported.

Preprint submitted to Elsevier Preprint *12 April 2000*

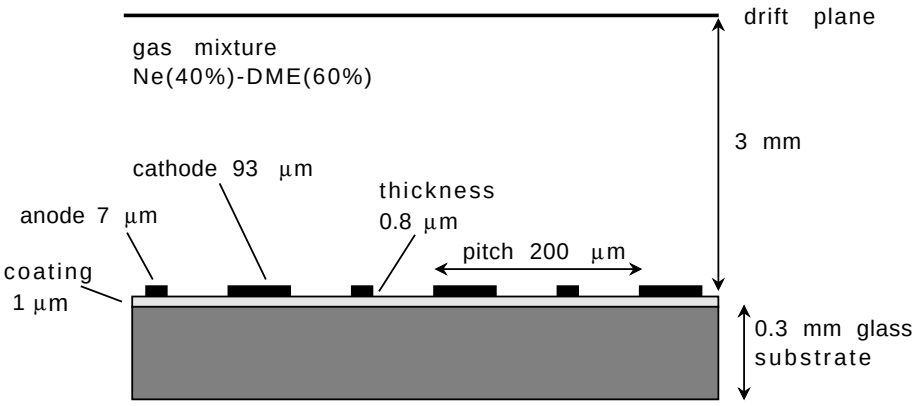

Fig. 1. Cross-section through an MSGC.

1 Introduction

The Micro-Strip Gas Chamber (MSGC) [1–4] is a position sensitive proportional counter whose operational principle is analagous to that of the Multi-Wire Proportional Chamber (MWPC), introduced by Charpak [5]. In the case of the MSGC, however, the sense electrodes are constructed using micro-electronics or thin-film techniques, see Fig. 1. Ionising particles traversing the drift gap produce ion-electron pairs. The electrons drift towards the anodes where the electric field is sufficiently high to induce avalanche multiplication and consequently a detectable signal. The feature size attainable using these methods is of the order of a few microns (compared with several hundreds of microns in the MWPC) and the detector has significant advantages in terms of spatial resolution and charge collection time.

The performance of an MSGC is strongly dependent upon several critical design parameters. These parameters have been optimised in the years since the inception of the detector and are fully discussed in the following section. Much of this research was driven by the need for a fast, high-resolution detector suitable for tracking applications in future high luminosity hadron collider experiments, e.g. the Compact Muon Solenoid (CMS) experiment at CERN's LHC facility. Recently it was reported that frequent induction of sparks between the electrodes of an MSGC can occur when the device is traversed by heavily ionising particles (HIPs) [6]. We describe a series of very extensive tests in which large numbers of MSGCs were exposed to such an environment (the πM-1 beam at PSI). The results of this work are reported and the steps required to overcome the sparking problem are discussed.

2 Optimised MSGC design parameters

In the course of the development work for CMS, several critical MSGC design features were studied in detail and refined to meet the required performance of the detector; here we summarise the choice of technologies and the reasons for these choices. Further details may be found in [7].

2.1 Substrate

Some of the positive charges produced in the avalanche process are inevitably deposited on the substrate instead of being directly collected by the cathodes or drift electrode. If these charges are not efficiently drained, they may accumulate and cause a local weakening of the electric field, resulting in a reduction of gain [8]. This effect will clearly be accentuated with increasing particle flux and is unacceptable for applications like CMS, where high particle rates (approximately 5 kHz/mm^2) are expected. Charging effects can be controlled by exploiting either the bulk or surface conductivity properties of the substrate. The conductivity should not however be *too* high, as then the electric field density close to the anodes is reduced and spread more uniformly in the gap between anodes and cathodes, approximating the parallel plate configuration [9]. This field configuration is more favourable to the development of streamers and requires higher cathode voltages to reach the needed gain. The best compromise therefore is to choose a substrate with the lowest possible conductivity compatible with the desired rate capability.
The industrial glass DESAG 263 has a bulk ionic conductivity and gives good rate capabilities if the detector electrodes are correctly biased (high drift field, $\approx$ 10kV/cm) [10,11]. However, some authors have reported long-term degradation of the detector performance for ionically-conducting glasses [12,13]. These effects are believed to be caused by ion migration within the substrate. Detectors with very good rate capabilities have been constructed using glasses in which the carriers within the bulk are electrons [14] (so-called *semi-conducting* glass). However, these glasses are heavy, fragile, expensive and not industrially available for large-area detectors.
An alternative solution is to deposit a thin layer of semi-conducting glass on the surface of an appropriate substrate. The bulk properties of the substrate are then effectively shielded and charging effects depend only on the surface conductivity of the thin layer. One approach is to use plasma deposition of diamond-like carbon [15]. This technique was initially very promising, but later tests showed that detector performance was unstable and liable to sparking in high-rate hadron beams, making such a solution unsuitable for LHC applications. Much better results were obtained by sputtering of a 1 μm layer of electronic conducting Pestov glass [16] onto a thin (300 μm) standard

glass (D263). The substrate surface conductivity was tuned to $\approx 10^{16}$ $\Omega/\Box$, a value known to provide good rate capability while at the same time maintaining tight concentration of the electric field lines around the anodes. This approach was the one adopted in the construction of our CMS *performance prototype* detectors.

2.2 Metallisation

Early MSGC designs used aluminium as the strip material, as this metal is commonly used in the microelectronics industry. However, it has been conclusively shown that this choice leads to rapid ageing of the detector (see, for example, [17]). It is thought that this is due to the fact that aluminium is an active metal which can react vigorously with the species produced in the avalanche plasma. Most studies have yielded good ageing results using chromium strips, but this metal has a relatively high specific resistance and is unsuitable for detectors with long (>10 cm) anodes read out by fast electronics [18]. The specific resistance must be lower than 50 Ω/cm to avoid position dependent attenuation of the signal and unacceptably high detector noise. A low resistivity metal with very good ageing properties [10,19] is gold, and our CMS prototypes were all constructed using this material.

2.3 Patterning

The anode width was chosen to be thin (7 μm) in order to provide high gain for the minimum possible bias voltage (approximately 520 V for a Ne/DME, 40/60 gas mixture). With a thin anode strip, the field gradient at the anode is very steep, resulting in efficient self-quenching of streamers which may otherwise develop into full discharges across the anode-cathode gap. The anode-cathode gap is 50 μm, requiring a cathode width of 93 μm.

2.4 Passivation

Certain regions of an MSGC, close to the electrode structures, have higher than average electric field strength which may induce the formation of streamers or sparks. An obvious example is the area close to the cathode ends, where extraction of electrons from the electrode metal may occur even at modest gains. Many researchers have passivated 'weak' regions of the electrode pattern with polyimide lines in an attempt to discourage charge extraction, with largely encouraging results. We have taken this idea a step further by passivating not just the cathode ends but also all cathode edges, using lines of

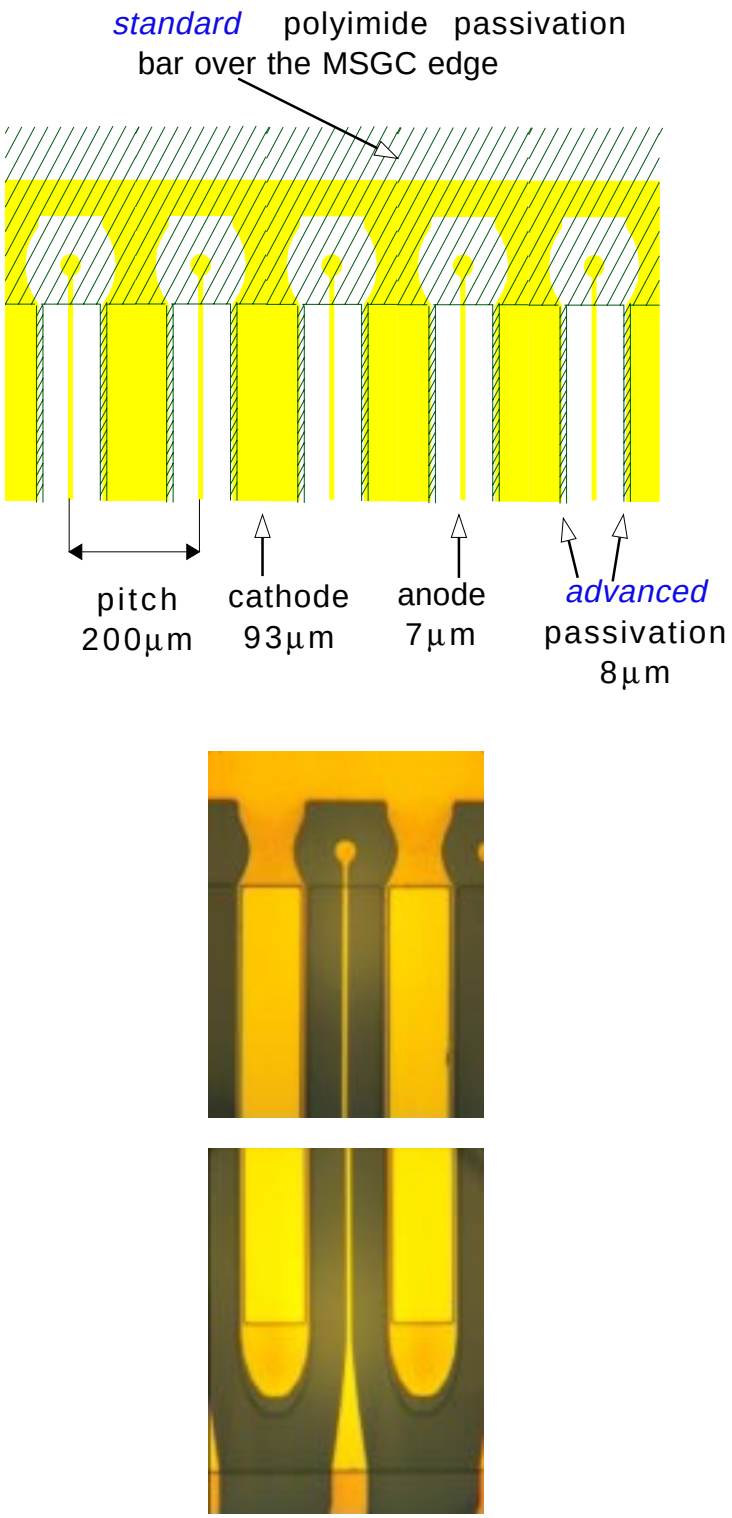

Fig. 2. Advanced passivation: polyimide line 4+4 μm wide, 2 μm thick.

polyimide 8 μm wide and 2 μm high, see Fig. 2. This approach, known as the *advanced passivation* solution, also reduces the probability of sparks induced by local lithographic defects along the cathode edge. Detectors built using

this technique have been shown to be significantly less prone to destructive discharges than devices operated without advanced passivation [20].

2.5 Resistors

The cathodes are ganged into groups of 16 and each group is connected to high voltage through a 2 MΩ protection resistor. This arrangement divides the overall detector capacitance and hence reduces the charge deposited on the electrodes in the event of a spark. The groups of 16 are collectively powered through an additional 5 MΩ resistor. No de-coupling capacitor is used in the circuit, again to minimise the available charge in case of a spark. A consequence of dividing the cathodes into groups of 16 is that there is a small (6 %) reduction in the signal current due to cross-talk (see [7] for further details).

2.6 Drift plane

Three options were considered: metallised glass fibre, carbon fibre or glass. Glass was rejected on the basis that it would add extra fragility to the detector; recent experience with carbon fibre drift planes indicated that there is a non-negligible probability of conductive carbon dust detaching from the drift, resulting in shorts between the detector electrodes. Metallised glass fibre was therefore chosen for our detectors. The spacer used to separate the drift plane from the substrate was made in molded PEEK (Poly-Ether-Ether-Keton). This material is radiation resistant, inexpensive and the frames produced were found to have good thickness uniformity.

2.7 Gas mixture

The chosen gas mixture was Neon-DME, 40-60 [21]. Di-Methyl Ether has the favourable property of having large primary cluster and total ionisation densities, 60 clusters/cm and 180 electrons/cm respectively. Its ionisation potential is quite low (10 eV). Running the chambers with 100 % DME would however require an unacceptably high cathode voltage (well above 600 V). This is because the mean free path of electrons in pure DME is rather small, each collision resulting in molecular excitations without ionisation. Neon has quite high excitation and ionisation potentials, 18 and 22 eV respectively. If the DME is 'diluted' with Neon, the probability of inelastic collisions is reduced, allowing the drifting electrons to acquire larger kinetic energies from the electrostatic field. This improves the efficiency of the ionisation process for DME, allowing sufficiently high gains to be achieved at cathode voltages as low as

520 V. Another advantage of using Neon, instead of for example Argon or Xenon, is that Neon is a poorer UV scintillator. This property, combined with the fact that DME is a strong UV absorber, serves to suppress the extraction of electrons from the electrode metals and therefore reduces the probability of after-pulsing and sparking. The Neon-DME mixture chosen provides a long voltage plateau length starting at a low working point bias [22]. The mixture is also advantageous in terms of detector ageing. The ageing process is mainly due to coating of the electrodes by polymers produced in the avalanche plasma. The formation of these polymers is known to be strongly catalysed by UV light and is minimised in 'UV free' mixtures. The operation of MSGCs at CMS required other properties from the gas mixture: a reasonably small Lorentz angle in the CMS 4 Tesla magnetic field and a high drift velocity to reduce pile-up effects within 2 bunch crossings of the LHC beam (50 ns). The gas mixture chosen has a 16^o Lorentz angle at 4 Tesla and a collection time of 53 ns at 10 kV/cm (3 mm gas gap).

3 Tests in a high-intensity hadron beam

The CMS performance prototypes were subjected to rigorous laboratory testing involving high-intensity X-rays, β and α sources. Long term ageing studies and investigations of the voltage margins were carried out and in all cases the detectors were found to perform well within CMS requirements (see, for example, [10,20]). Equally successful tests were performed at various test-beam facilities, which included tracking studies to assess the spatial resolution and hit detection efficiency of the chambers [23]. These beam tests generally made use of relatively high momentum particle beams (several GeV/c) with light duty cycles (e.g. 5 % at the CERN T10 area).
In the past few years concerns have been raised about the effect on MSGC performance of highly ionising nuclear fragments (HIPs), produced by the interaction of hadrons with the chamber structure. It was suggested that such fragments, passing close to a high-field region of the detector, could induce streamers or spark activity, significantly shortening the voltage plateau [24].
A study of the energy distribution of the high intensity background forseen at LHC and the cross-section for the production of nuclear fragments has suggested that the best simulation of LHC could be obtained with low energy pion beams. The πM-1 test beam area at the Paul Scherrer Institute (PSI) was therefore chosen to investigate this effect. This facility provides an almost continuous beam of 350 MeV/c pions and protons; operating at a particle rate of around 6 kHz/mm^2 over a 100 cm^2 area, the chambers were exposed to harsh conditions comparable with those expected at the CMS inner MSGC radius. In this section we describe the PSI set-up and experimental programme and report the results of the latest, and most exhaustive, series of tests performed.

These tests constituted an official CMS *Milestone*.

3.1 Quality control

The Milestone was not simply a test of the ability of MSGCs to withstand CMS conditions; it also provided a framework in which to assess the capabilities of the industrial production lines and the effectiveness of our quality control and data recording procedures. The detectors had to pass two main quality control phases before being accepted for the PSI tests. Firstly the basic substrates with patterning, as received from the manufacturer, were optically and electrically tested. Plates passing this stage were assembled into fully operational chambers which underwent rigorous assessment in a dedicated test station, consisting of a full data acquisition system triggering on betas from a radioactive source.

Eighty (80) plates were produced by CeTeV (Centro Tecnologie del Vuoto, Carsoli, Italy). The dimensions of the active area on each substrate was approximately 10× 25 cm. Each active area comprised 2 detectors with 12.5 cm strip length. The strip capacitance was measured for each substrate to identify broken anodes, broken strips having a capacitance significantly lower than the mean. The data from this assessment are presented in Fig. 3 (upper plot). Optical inspections of each plate served as an additional check of the broken anodes and also identified additional lithographic anomalies such as edge defects and shorts, see Fig. 3 (lower plot). Grouping all defects together (Fig. 4), we judged 75 (94 %) of the 80 substrates to have fewer than 3 % defective strips, and 59 (74 %) with fewer than 2 %.

Forty-four substrates were shipped to Laben SpA (Florence, Italy) where they were assembled into detectors (this number was reasonable considering the Milestone requirement of 32 working chambers and the limited time available for construction). The assembly process involved gluing the drift plane and spacer to the substrate, attachment of gas connections and high voltage connections, mounting of the electronics hybrid and wire bonding of the anode read-out strips to the hybrid. Strips identified as being defective from the electrical and optical inspections were not bonded. High voltage was supplied to the cathodes by means of a second hybrid, mounted below the electronics hybrid, see Fig. 5. The distance between anode (at ground) and cathode (at high voltage) bonding pads on the substrate was just 200 μm, and the pattern of bonding was carefully studied to avoid shorts. This was achieved by keeping all bonds consistently parallel and by providing vertical separation between anode and cathode bonds (short, low cathode bonds; longer, higher anode bonds). A fully assembled detector module is shown in Fig. 6. The total instrumented area of the 44 modules was 1 m^2, equivalent to 1 % of the surface of the CMS barrel, and was assembled in only four weeks.

The chambers were tested, four at a time, by irradiating them with a strong

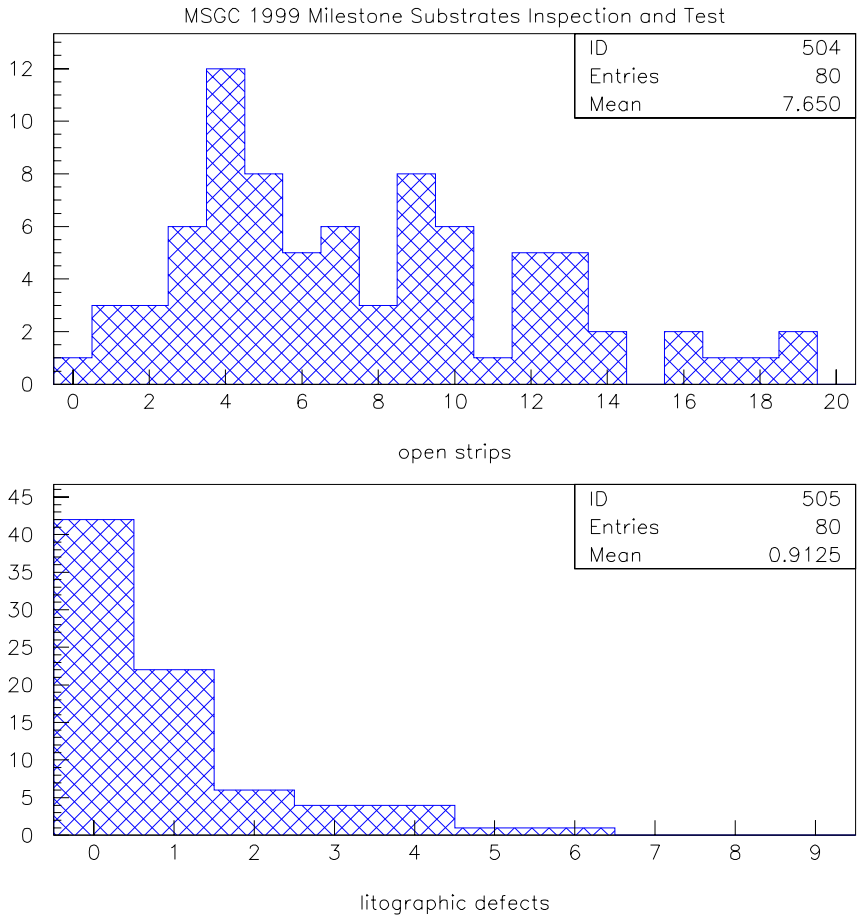

Fig. 3. Distribution of open strips (upper plot) and other lithographic defects (lower plot) for the 80 substrates received from CeTeV.

beta source (^{106}Ru, 10^5 Bq). All 512 strips from each of the chambers were read out using a VME-based data acquisition system identical to the one later used at PSI (see section 3.3). In-house analysis software was used to construct several important diagnostic plots, in particular: landau and signal-to-noise distributions; hit position distributions; cluster width; mean cluster area as a function of hit position. The latter plots gave an indication of the gain uniformity across the chamber. The S/N histograms were used to estimate the working point voltages for each detector. Data was also acquired without the beta source in position (a so-called *pedestal run*), allowing the noise for each individual strip to be evaluated. Broken or unbonded strips have a lower than average capacitance and therefore lower than average noise. The first pedestal run after chamber assembly (before applying voltage) provided a valuable cross-check of the previous quality control steps.
After establishing the working point, the voltages were raised to give a S/N approximately 50 % above the working point value. The chambers were then left in this condition for a period of several hours. During this time, the current drawn by the cathodes was continuously monitored by the DAQ allowing spark activity to be readily detected. Pedestal runs identified any additional

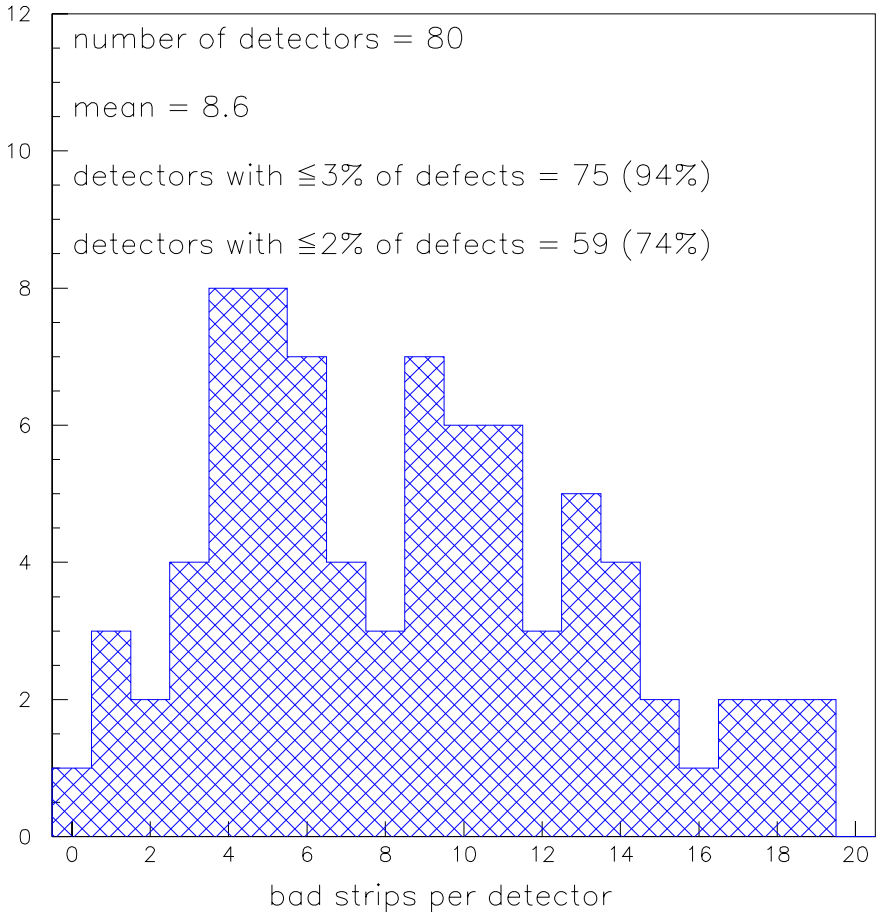

Fig. 4. Distribution of all detected lithographic defects.

broken strips. Of the 44 assembled chambers, only 3 were rejected during laboratory testing, leaving 32 for the PSI Milestone and 9 spares.
All important quality control information (initial number of defects, working point voltages, strips broken after applying voltages, etc.) was recorded in a dedicated database.

3.2 Experimental layout

The chambers were mounted on aluminium plates, the central regions of which were removed to minimise multiple scattering of the beam. These plates also supported motherboards for the electronics and a services panel on which all of the needed connectors were mounted (high voltage, low voltage for electronics, gas connections, electronics control signal inputs and outputs, video cable connections for signals from the detector). Two large precision engineered crates were constructed each with 16 slots into which the chambers on their aluminium support frames could be placed vertically, see Fig. 7. The distance between substrates was 4 cm and the sense electrodes were generally

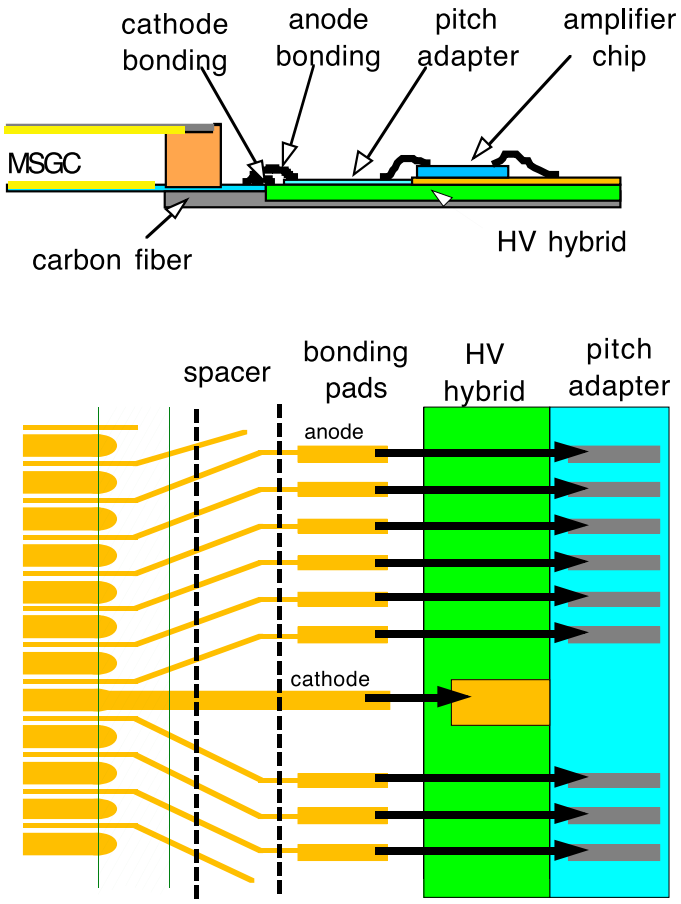

Fig. 5. Layout of electronics and high voltage hybrids.

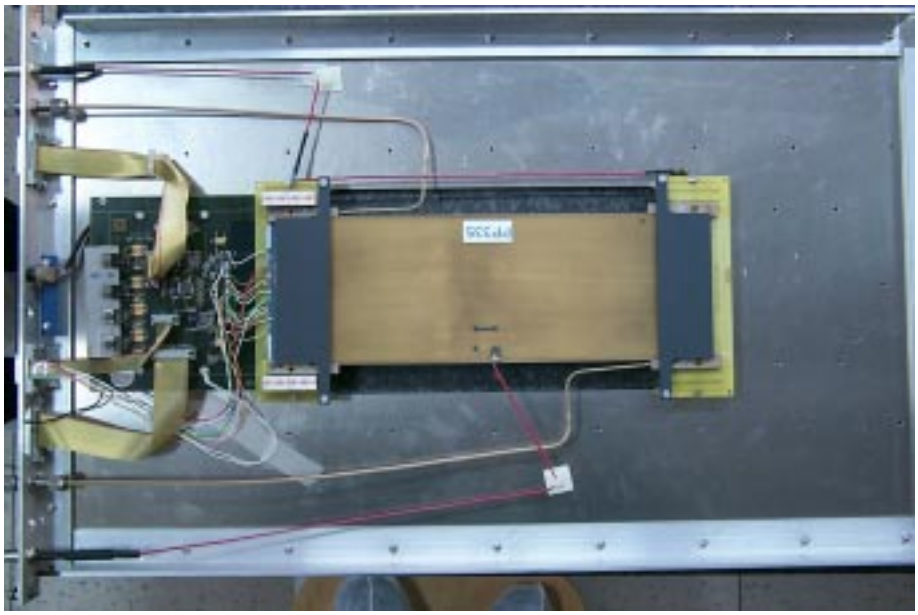

Fig. 6. A fully assembled MSGC module of the type used in the PSI tests.

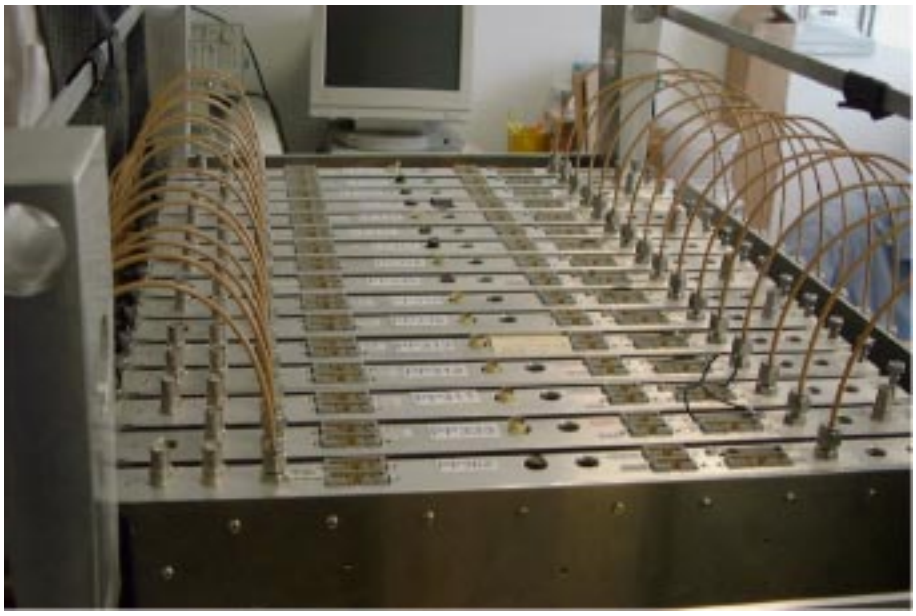

Fig. 7. Each of the large precision engineered crates could accept up to 16 MSGCs.

vertical; however for 8 of the chambers the detector modules were mounted on the support frames such that their strips were at a small stereo angle to the vertical ($\tan(\alpha) = 0.1$). This modular system was advantageous in several ways; most importantly, setting-up time in the PSI beam area was minimised, since the 32 chambers were positioned in the beam simply by aligning the two boxes. Gas was supplied to the crates through two separate stainless steel lines; mass flow meters were used to monitor the Neon/DME ratios in each of these lines. For each crate, the gas mixture was fed to the chambers through 16 parallel needle valves which allowed independent flow rate adjustment. On leaving the chambers the gas passed through individual bubblers and was then expelled into a common exhaust line. The renewal rate of the gas mixture for each detector was approximately 5 chamber volumes per hour.

A schematic layout of the experiment is shown in Fig. 8, in which the beam direction is from left to right. The Milestone tests described here were performed on MSGCs designed for the barrel region of CMS, see [7]. This work was conducted in parallel, and in close collaboration with, groups involved in a similar Milestone for the forward region of CMS. The two boxes containing the barrel MSGCs were placed on either side of the 'forward' detectors. The chambers were sandwiched between a set of trigger scintillators designated LIF, LIB (low intensity front/back, 10 cm $\times$ 10 cm) and HIF, HIB (high intensity front/back, 1 cm $\times$ 5 cm). An additional small counter, HIM (high intensity middle), was placed between the forward detectors and the second barrel crate.

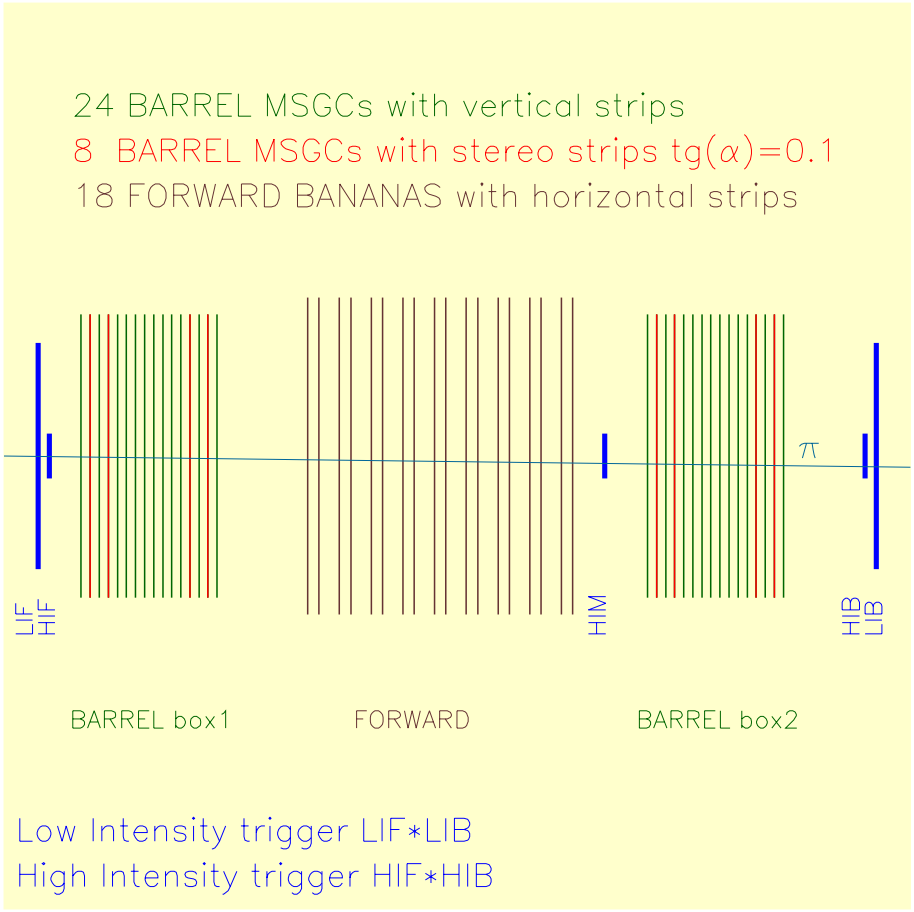

Fig. 8. PSI test beam set-up.

3.3 Data acquisition system

Each detector was equipped with four Premux-128 chips, which were used to amplify and multiplex signals from the 512 anode strips. A detailed description of this chip may be found in [25]. The total number of strips to be read out for the barrel system alone was 16384.
Digitization of the signals was performed by Caen V686 Sirocco Flash-ADCs [26]. Triggers at high intensity were provided by the coincidence of the two crossed scintillators HIF and HIB, with an equivalent area of 100 mm^2. Read-out synchronization was achieved using a SEQSI sequencer card [27]. Overall control of the VME modules was via dedicated software running on a Creative Electronics Systems (CES) RIO processor [28].
A second VME crate was provided for slow control. Custom-built (CERN) pico-ammeters were cabled in series with the cathode high voltage supplies for all of the detectors. The analogue outputs of the pico-ammeters were digitized with LeCroy 1182 ADCs in the slow control crate. The sampling rate of 500 Hz was sufficient for the efficient detection of discharges (the re-charge time constant of the MSGC is around 30 ms). The slow control system also

included scalers for automatic recording of the particle rate through all of the scintillators. The modules in the crate were controlled by software running on a CES FIC processor [28].
Overall control of the data acquisition was by means of custom software running on a Linux-based PC. Data communication with the VME processors was managed using TCP/IP sockets. Data collected during the test were automatically written to tape using a DLT-2000 drive. An on-line monitoring program ran on a second PC; communication with the event builder was again achieved using the TCP/IP protocol. The data acquisition system described above was provided by the IPN-Lyon HEP group.

3.4 Experimental procedures

After installation of the chambers and data acquisition system, a pedestal run was performed in order to record the condition of the detectors prior to applying voltages. With low intensity beam, the voltages on all of the chambers were raised until the S/N values were slightly below the working point. The final preparatory step was to check and adjust the timing of the detectors so that the Premux chips were sampling at the signal peak. This was achieved by altering the length of a common delay cable incorporated into the trigger electronics and identifying the common delay value corresponding to the maximum landau peak position for each chamber. The timing for each chamber was then individually adjusted if necessary by adding or removing cable between the trigger card and the Premux motherboard. In practice, variations in timing between detectors were negligible.
All of the chamber voltages were then adjusted to set the detectors to their individual working point gains. The beam magnets and collimators were adjusted to provide a high intensity π^+ beam with a proton contamination of a few percent, well centred along the axis of the test bench. The beam parameters were well known from our previous experience at PSI [29]. The particle rate maintained on the first high intensity counter was approximately 6 kHz/mm^2. The high intensity running period was divided into 3 phases: one week of 'hardening', during which previously undetected small lithographic defects were expected to 'burn out'; three weeks of continuous high intensity running with limits imposed on the acceptable number of strips lost (the official 'Milestone' period); one week in which voltage margins would be studied by raising the S/N above the working point values. The high intensity rate was maintained at all times, except for two periods of approximately one hour every day when pedestal runs were taken. A short low intensity run (approximately 300 Hz/mm^2) was also made during these times, triggering on the coincidence of the LIB and LIF counters, allowing a check of the S/N of the chambers (at high intensity the S/N was artificially high due to pile-up effects). In addition to these 'survivability' tests, tracking software was written

to accurately evaluate the hit detection efficiency of the chambers and the 2-D reconstruction capability of the system was investigated using information from the stereo modules.

4 Results

4.1 Milestone definition

The milestone for the Barrel was officially defined as follows. Twenty-five MSGC detectors (12800 strips) with advanced passivation should be irradiated at the PSI πM-1 facility at the LHC rate for a total integrated time of 15 days (360 hours). The milestone was to be considered successful if after that time fewer than 30 new broken strips were detected. This would extrapolate to a 10 % strip loss after 10 years of LHC running, resulting in 5% of the overall detector area with reduced resolution. Twenty-five of the 32 detectors installed at PSI were identified beforehand for the milestone. However, non-milestone detectors showed no significant differences in performance and in what follows we refer to the full set of 32 chambers.

4.2 Beam intensity monitor

The scaler counts for each of the scintillators were recorded by the DAQ. The counts from HIF, which was switched on even during low intensity runs, were used to estimate the total integrated high intensity time, see Fig. 9. For the full 5-week high intensity period this time was 493 hours, while for the 3-week milestone phase the corresponding value was 376 hours, comfortably in excess of the required 360 hours. The two large gaps visible in Fig. 9 coincide with machine maintenance periods for the PSI accelerator.
A more careful study of the average particle rate on each of the 32 chambers was performed later. We used a random trigger during a high intensity run to determine the true shape of the beam in each detector, unbiased by the scintillator shapes. An example for the first chamber of the first crate is shown in Fig. 10. At the time the data were taken, the rate on HIF (1 cm wide, centred with respect to the MSGCs) was 6.2 kHz/mm^2. The distribution in Fig. 10 is normalised to this rate. Integrating over the area of the distribution allowed an average value of 4.2 kHz/mm^2 to be calculated. Knowing the gain of the chamber and the number of primary electrons generated for each of the incident pions, the average overall signal current could be estimated; this value was in very good agreement with the measured value (cathodes plus drift).
A similar exercise was performed for all of the chambers; comparison of the

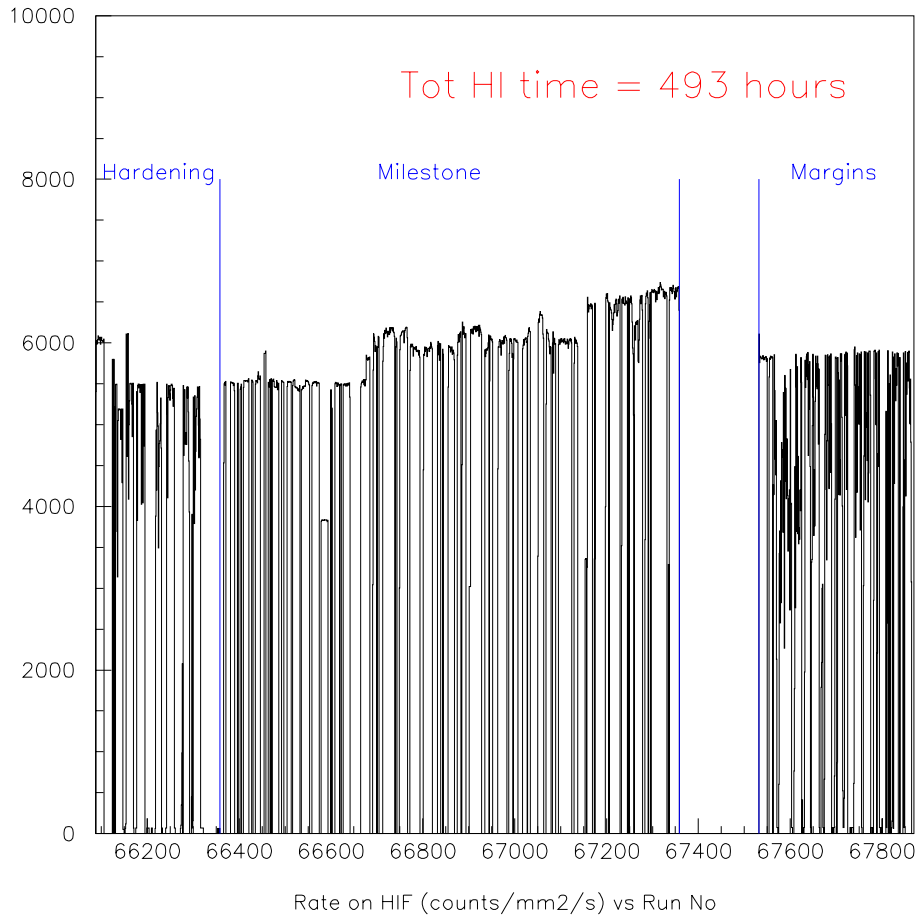

Fig. 9. Particle rate on HIF as a function of run number, covering the whole 5 week high intensity period.

beam profiles taken with the random trigger allowed us to characterise the variation in rate as a function of position along the beam, see Fig. 11. The plot shows the peak rate for each detector; using the method described above, these values were translated to average rates. Given that the exposure for the milestone period was 376 hours, the overall average fluence could then be calculated and was found to be 3.4×10^{11} pions/cm^2. It has been estimated [7] that the total hadron fluence for the innermost MSGC layers at CMS, after 10 years of LHC running, would be 10^{13} cm^{-2}. The ratio of this value to the average fluence for the milestone period is 29.

4.3 Detector stability

The low intensity hit position distributions (beam profiles) for all 32 chambers are displayed in Figs 12 and 13. The plots reflect the very low percentage of defective strips reported in section 3.1. It should also be noted that the beam extended over the whole active of the detectors, including the spacers and

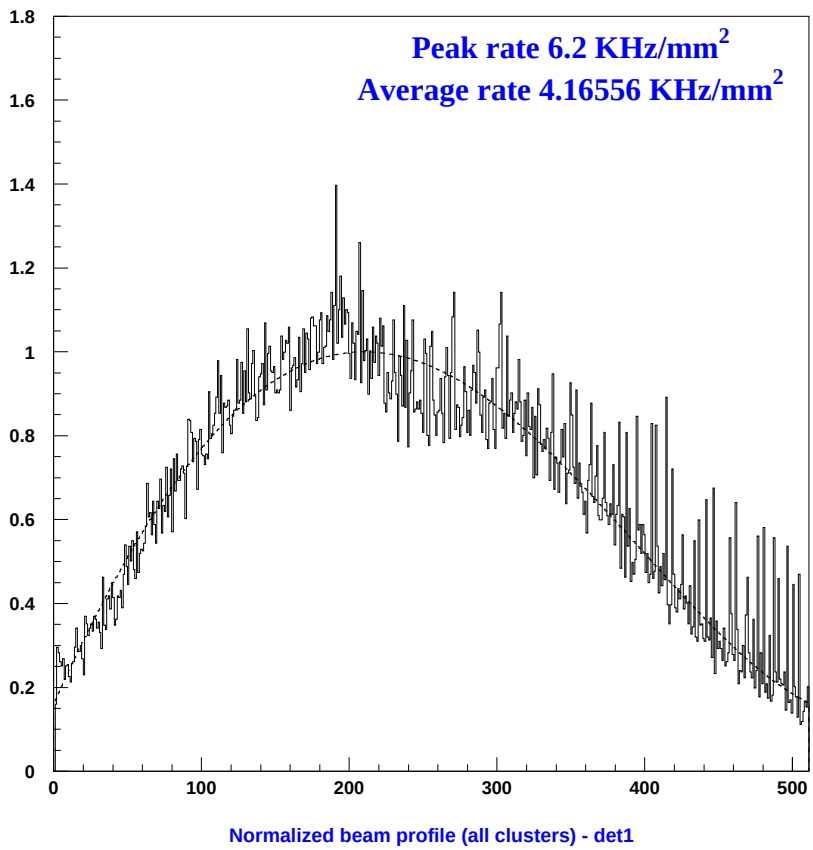

Fig. 10. High intensity beam profile (random trigger) in first chamber of crate I.

other non-active areas; this situation is in contrast to many previous tests using sources or x-ray generators, in which usually only a relatively small area of the detector could be irradiated at high intensity.

The S/N distributions built by the online monitor analysis program could be quickly and easily fitted and the peak value plotted as a function of run number; an example for one chamber from each crate is plotted for the complete milestone period in Fig. 14. The S/N definition used in this plot, and throughout the rest of the paper, is that described in [7] [1] . The points are clearly divided into two horizontal bands, corresponding to low intensity runs (lower band) and high intensity runs (upper band). This is a result of pile-up phenomena at high intensity. The effect was much more pronounced for the chamber in the first crate, which was closer to the beam pipe window. It was estimated that multiple scattering and beam divergence caused the particle rate in the last chamber to be reduced by a factor 4 compared to the rate in the first detector crossed by the beam.

A more careful analysis was performed for the low intensity data using an off-

[1] If the signal charge is deposited over n strips, and the signal on each of these strips is denoted by Q_i with corresponding noise σ_i, then $S/N_{tdr} = \Sigma_{i=1}^{n} Q_i / \sqrt{\Sigma_{i=1}^{n} \sigma_i^2 / n}$

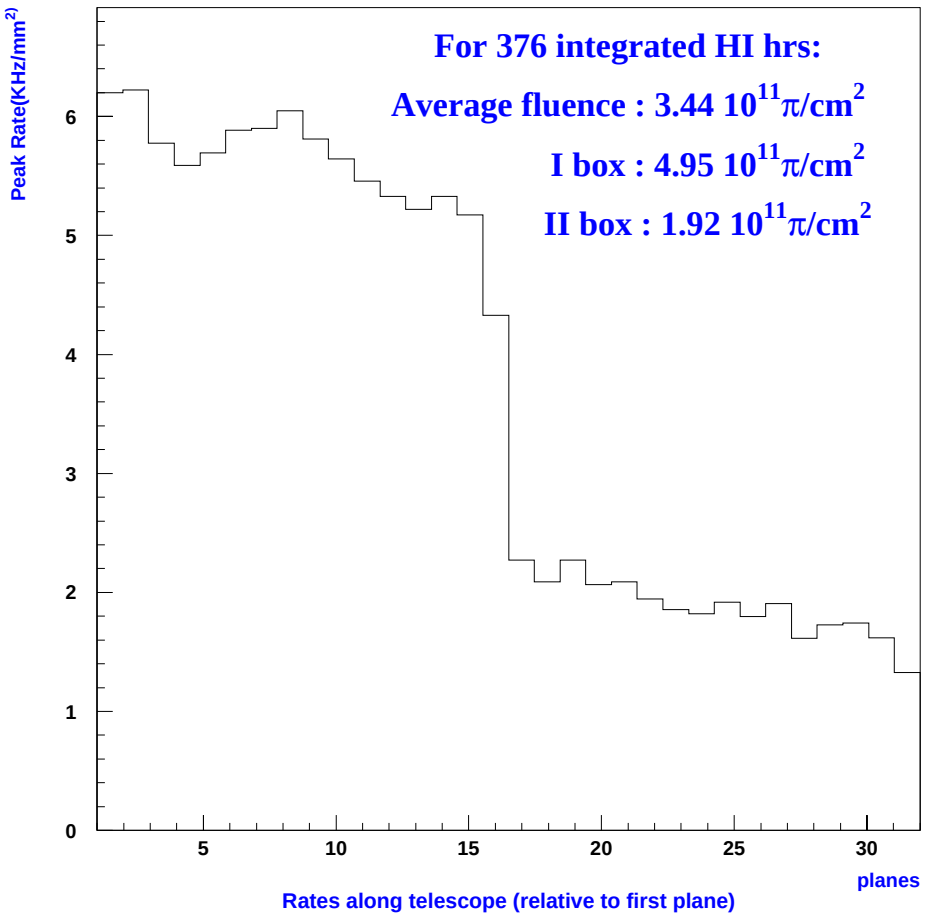

Fig. 11. Particle rate as a function of detector position along the beam. The sharp step corresponds to the transition from the first detector box to the second (intervening space occupied by chambers from the 'Forward' groups).

line software package. A feature of this analysis is that a correction is made for the signal 'lost' due to cross-talk (see section 2.5). The S/N was averaged over all 32 chambers and is plotted for the milestone period in Fig. 15. The lower horizontal line indicates the 'working point' S/N value of 28. It is well established that the voltages required to achieve this S/N with Premux electronics correspond to those necessary to achieve 98 % hit detection efficiency with the APV electronics which will be used at CMS; we discuss this point in more detail in section 4.7. It is clear from Fig. 15 that the average S/N was above this limit for the entire milestone period. Furthermore, there is no evidence of any gain reduction due to ageing effects (the short-term variations in S/N visible in the plot are most likely due to changes in atmospheric pressure). The distribution of S/N values about the average, for a typical point in the milestone period, are displayed together with the corresponding cathode voltage distribution in Fig. 16.

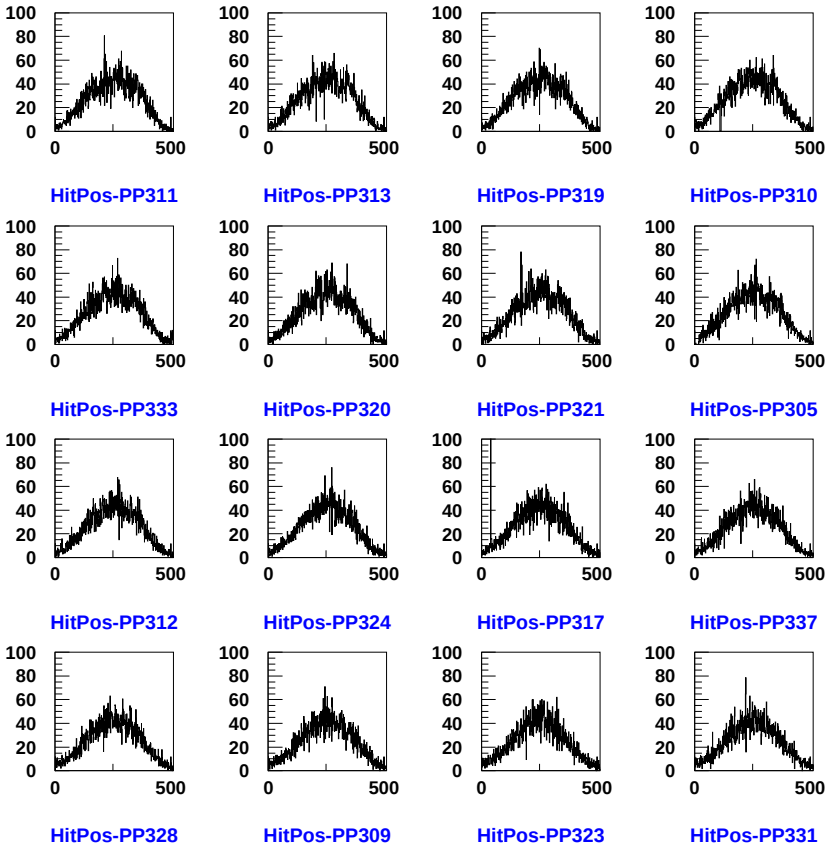

Fig. 12. Beam profiles for chambers in crate 1.

4.4 Voltage margins

During the final week of high intensity running, the voltage margins of the detectors were studied as follows. Eight of the 32 chambers were used as a reference, and kept operating at the normal working point S/N. The cathode voltages of the other 24 chambers were raised to give an average S/N ratio of 39, 1.4 times the working point value of 28. For 12 of these chambers, this S/N value was maintained for the whole margins period. The cathode voltages on the other 12 chambers were further raised after a period of about 2 days to achieve a S/N of 1.7 times the working point value. After a further period of around one and a half days, six of these 12 were studied at a S/N of 2.4 times the working point, for an integrated high intensity period of approximately 24 hours. The distribution of S/N values as a function of detector number are summarised in Fig. 17 and the cathode voltage distributions are shown in Fig. 18. In Fig. 19 we summarise the variation with time (run number) of the S/N values, averaged over each of the different sets of detectors. No serious deviations of the gain from the average values were observed during the margins study.

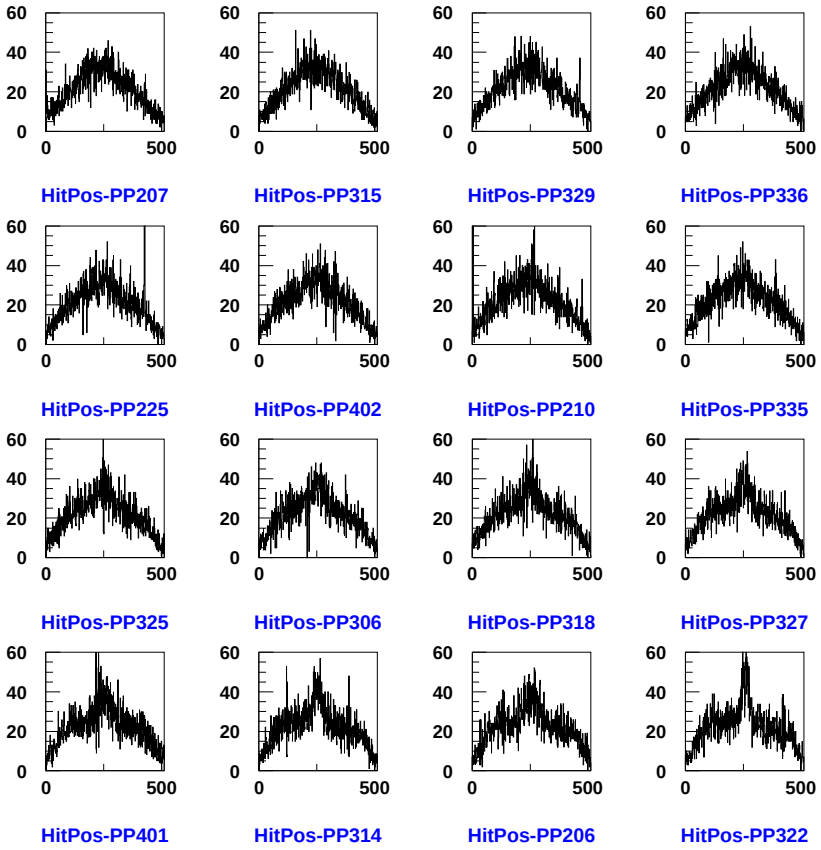

Fig. 13. Beam profiles for chambers in crate 2.

4.5 Strip loss summary

The condition of the detectors was continuously monitored by examining the data from the twice-daily pedestal runs. The noise distributions were carefully compared with reference data taken at the beginning of each of the three experimental phases (hardening, milestone period, voltage margins period). Any channel losses could easily be identified by a reduction in noise for the affected channel. The most convenient way of comparing the noise values of the strips within a particular chamber with those from the reference pedestal runs was to take the ratio of the two distributions. The ratio was close to 1.0 for normally operating strips and below this value for broken strips or dead electronics channels. We defined a threshold value of 0.9 for this ratio in order that a strip be identified as dead.

A summary of the strip losses during all stages of this project is given in Table 1, and a graphical representation for the whole high intensity period is shown in Fig. 20. A total of 4 out of the 16384 channels were lost during the hardening phase; 3 were broken in the 3-week milestone period; one further channel loss was detected during the margins study. The integrated high in-

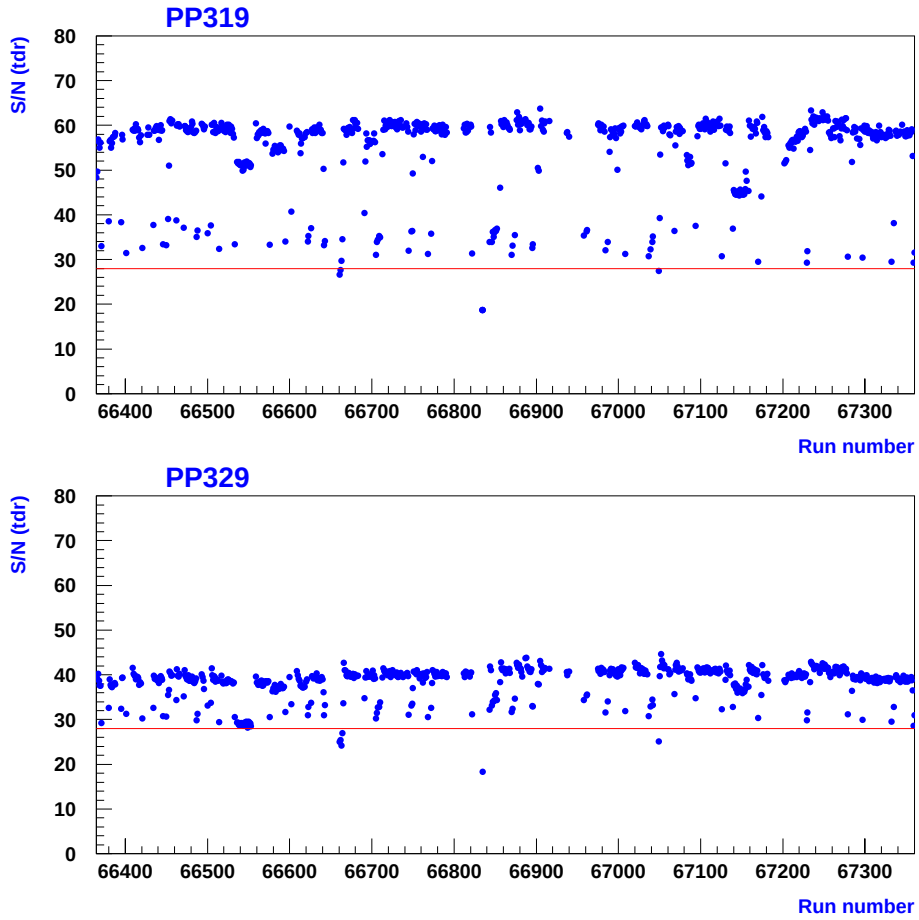

Fig. 14. Online monitor S/N peak position as a function of run number for typical chambers from crate 1 (top) and crate 2 (bottom). The milestone working point S/N of 28 is indicated by the dotted horizontal lines. The separation of the data points into horizontal bands is as a result of pile-up effects at high intensity; the bands are closer together in the second crate where the high-intensity rate was lower.

nb. of detectors	25 (milestone)	32 (tested at PSI)	41 (tested+spares)	44 (produced)
total nb. of strips	12800	16384	20992	22528
nb. of unbonded strips	111 (0.9%)	161 (1%)	215 (1.02%)	230 (1.02%)
lost chans. after lab test	129 (1.01%); +18	194 (1.18%); +33	293 (1.4%);	350 (1.55%)
lost chans. at PSI (setup phase)	131 (1.02%); +2	201 (1.22%); +7		
lost chans. at PSI (hardening phase)	132 (1.03%); +1	205 (1.25%); +4		
lost chans. at PSI (milestone)	134 (1.05%); +2	208 (1.27%); +3		
lost chans. at PSI (margin phase)	134 (1.05%); –	209 (1.28%); +1		

Table 1
Summary of all strip losses for each phase of the PSI investigation. The incremental loss is shown at the right of the columns while the cumulative value is shown on the left.

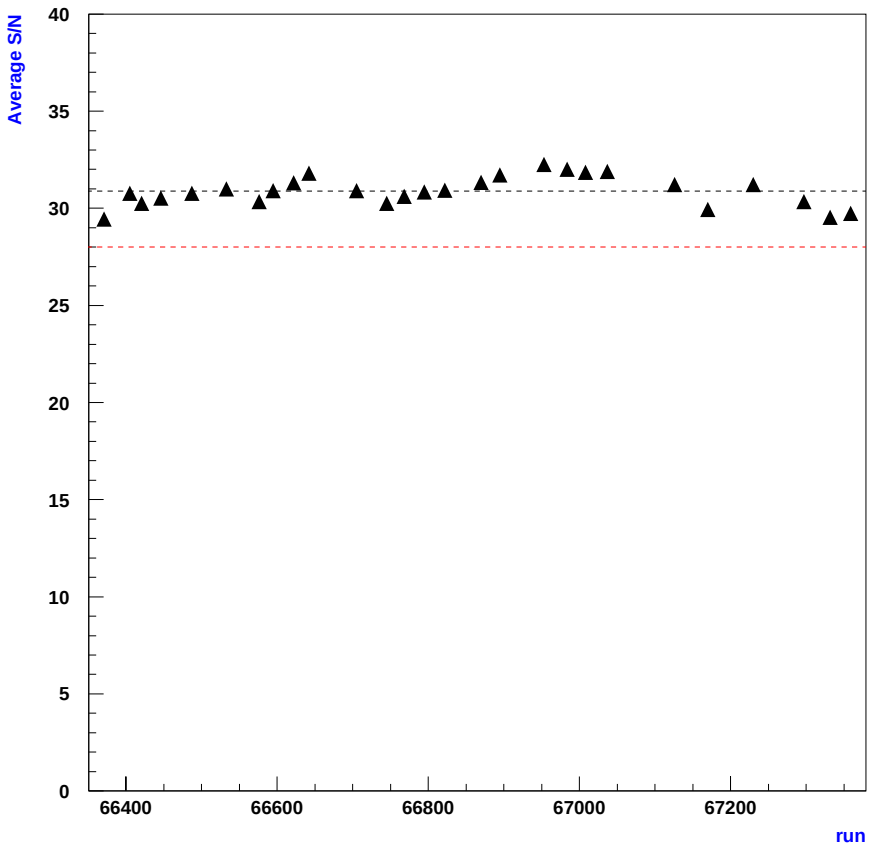

Fig. 15. Off-line S/N peak position averaged over all chambers for the milestone period.

tensity times for these periods were 43, 376 and 74 hours respectively. We can extrapolate to the estimated loss of strips after 10 years of LHC running using our knowledge of the average fluence during the milestone period compared with the expected 10-year fluence at CMS (see section 4.2). The extrapolation factor of 29 yields a value of 0.5 % for the expected 10-year strip loss (3/16384 $\times$ 29 $\times$ 100 = 0.5 %), 20 times lower than the Milestone requirement.

4.6 Spark rate study

The online monitor was used to carefully observe the behaviour of the detector cathode currents during the test period. Off-line analysis of the current data was later performed. The software identified spark candidates and appropriate cuts were then applied, including cuts on the integrated charge and on re-charge duration (calibration of the current measurement chain was performed in advance of the tests, to establish the relationship between ADC counts and absolute charge). The results of the off-line analysis are summarised in Fig. 21.

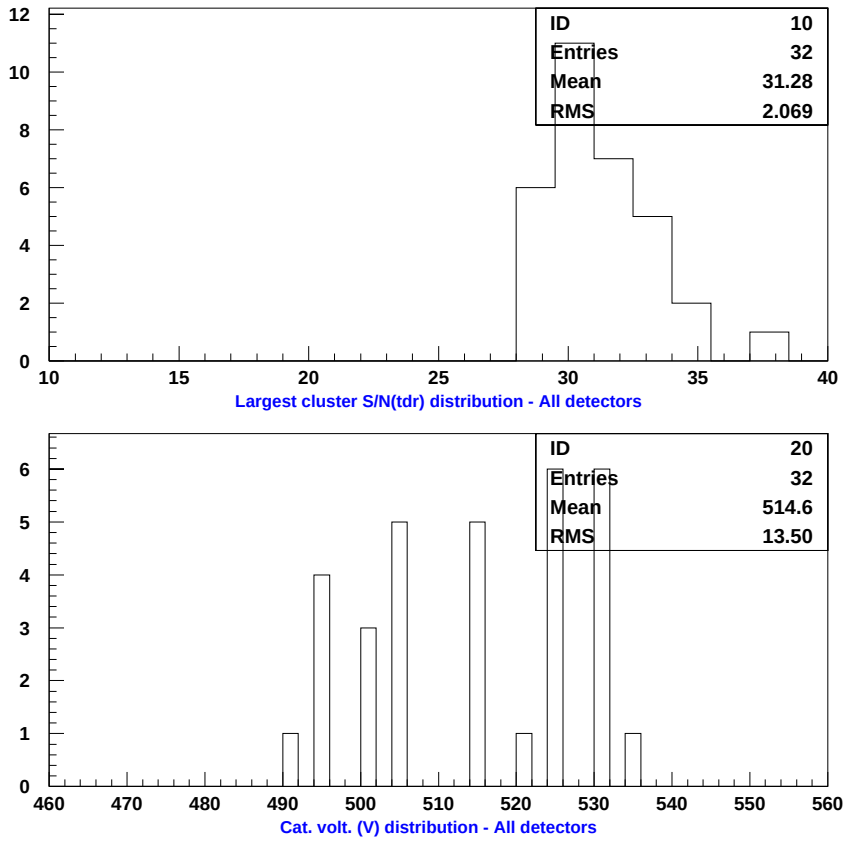

Fig. 16. Distribution of S/N values and the corresponding cathode voltage distribution for all 32 chambers at a typical point during the milestone.

The upper plot shows that the total charge within events identified as sparks fall into 3 distinct zones. The most populated distribution is centred around the charge corresponding to discharge of a full high voltage group (16 strips). Other, far more rare, events are located in a distribution whose peak has a value approximately twice that of the main peak. These events correspond to the discharge of two adjacent cathode groups to the intervening anode. Several entries are also present below the main distribution and can be interpreted as partially quenched streamer events.
The lower plot in Fig. 21 shows the average spark rate in the detectors in the two different crates as a function of run number. The spark rate was always higher in the first box, where the particle rate was higher, but in both cases was low from the beginning (fewer than 1.5 sparks per chamber per day). In both boxes, the rate decreased with time, reaching a minimum of 1 spark/chamber/day in the first box and 0.7 sparks/chamber/day in the second box at the end of the milestone period. The average spark rate in both crates increased only very slightly as the voltages were increased during the margins study but was always well below the initial rate.

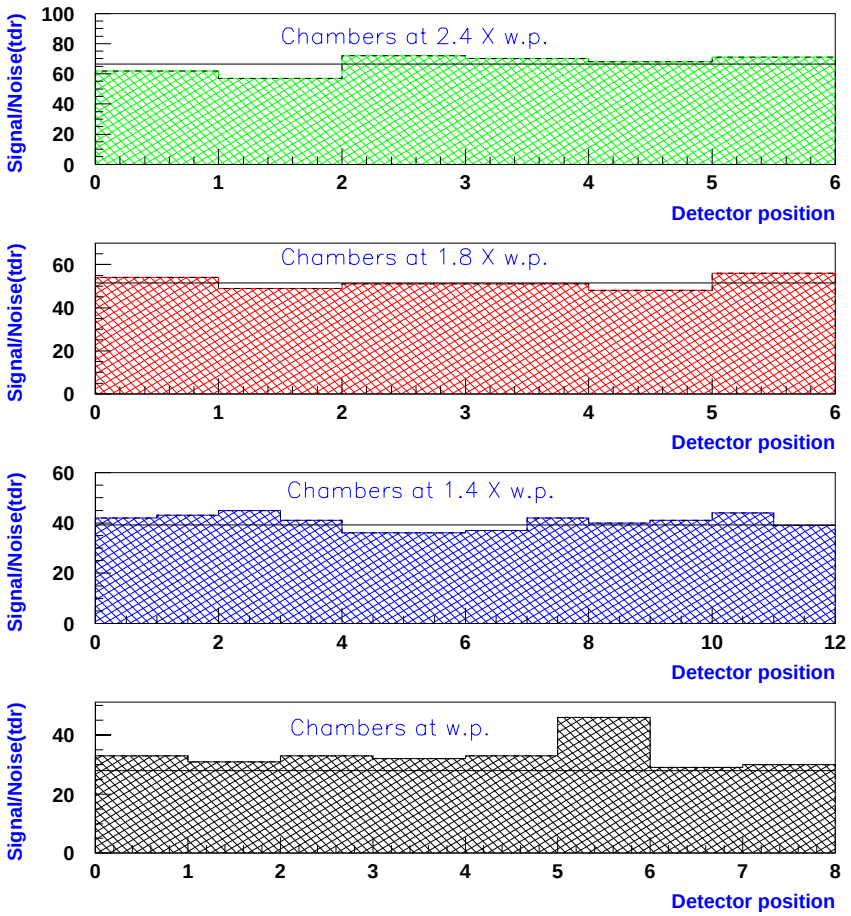

Fig. 17. Distribution of average S/N values as a function of detector number for the voltage margins study.

4.7 Tracking and hit detection efficiency

The tracking potential of the PSI set-up, with its 32 high-resolution points, is manifest. The main limitation was introduced by multiple scattering. A crude but instructive picture of tracks at low and high intensity were immediately available from the on-line monitor, see Fig. 22. The plots display the pedestal subtracted data for single events for all 32 chambers. Noise-free tracks could clearly be distinguished simply by applying a single blanket cut of 3.5 σ of the electronics noise over all of the data. This fact provides reassuring confirmation that system noise, e.g. pick-up and any other non-Gaussian tails, had been eliminated from this large set-up.
In-house software was written to provide more sophisticated track re-construction. In order to avoid the inevitable large number of out-of-time tracks present at high intensity, we concentrated our efforts on the analysis of low intensity data. A sub-set of 11 detectors from the first box were used to construct tracks; use of the data from chambers further downstream was limited by multiple scattering.

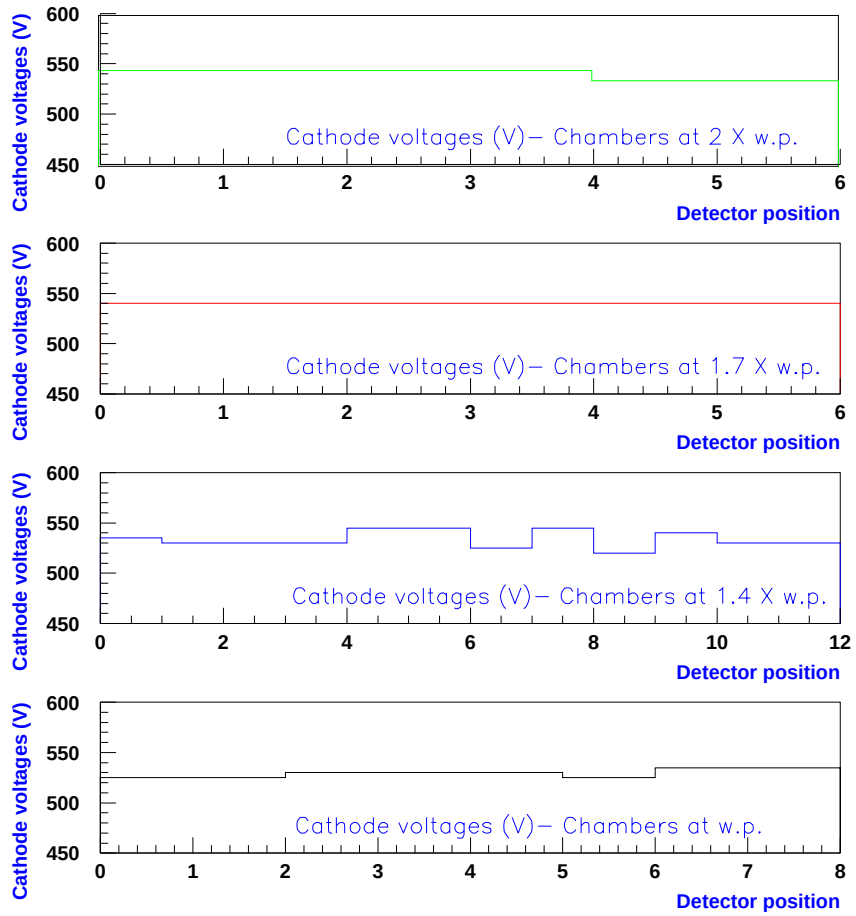

Fig. 18. Distribution of cathode voltages during the margins study.

A critical result from the tracking study was the evaluation of the hit detection efficiency of the MSGCs. In Fig. 23 (dots) we plot the efficiency calculated by the tracking software for a typical detector as a function of the cluster seed threshold [2] at a S/N value of 12.4. As expected, the detector efficiency increases as the seed threshold is decreased. However, the threshold cannot of course be reduced indefinitely since for very low thresholds we are unable to distinguish the signal from noise. This point is further illustrated by the second set of curves in Fig. 23 (triangles), which show how the average number of clusters in a single event depends upon the seed threshold. We see that a lower limit for an acceptable threshold is in the range 3.5 to 4.0 σ.

[2] The analysis program keeps a record of the noise for each strip of each chamber, calculated from the last pedestal run. For a cluster to be considered as a hit candidate in the detector under test, the signal on at least one strip in the cluster must be higher than a specified multiple of the standard deviation of the noise for that strip. We refer to this multiple as the *seed threshold*. To build the cluster a second, lower, threshold is introduced, which must be exceeded by the signals on the remaining strips in the cluster. In the plots we refer to this cut as the *single strip threshold*.

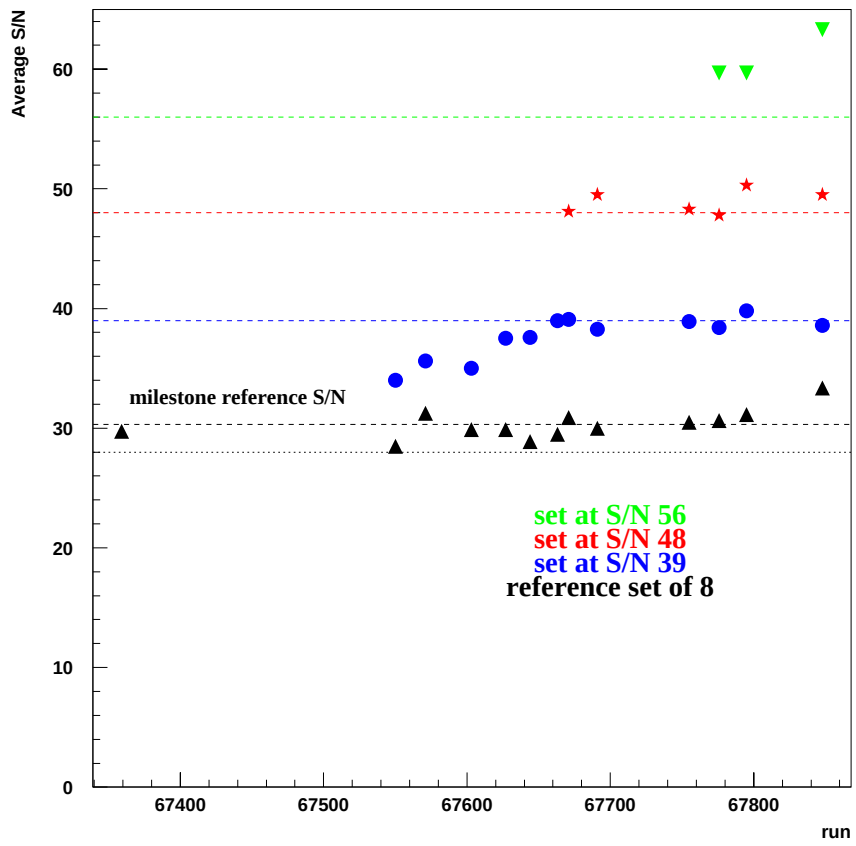

Fig. 19. Variation of average S/N with run number (margins period) for each of the different sets of detectors.

The plot of efficiency versus seed threshold can be made for various values of signal-to-noise. This study was also done on a previous occasion at PSI and the results are presented in Fig. 24 (upper plot). Using the data from this graph with seed thresholds of 3.5 and 4, we can construct the more useful graph of efficiency as a function of S/N, see Fig. 24 (lower plot). The results from the Milestone run are shown together with the data from the older study. From this graph we infer that to achieve the 98 % efficiency required for CMS, using a seed threshold of 4, the necessary S/N is 13. Operating the chambers at this S/N at PSI, *where Premux electronics were used*, the cathode voltage was approximately 470 V. For CMS, APV electronics [7,30] will be used, for which the noise and ballistic deficit are expected to be higher. It is predicted [7] that for the same voltage settings, the S/N will be reduced by a factor 2.2 at CMS because of these effects. To make a fair comparison using Premux electronics requires that the detectors be run with a signal-to-noise ratio 2.2 times higher than 13, i.e. at least 28. The chambers evaluated at PSI for the Milestone test were always operated at a S/N comfortably in excess of this value (average 31, see section 4.3). It is interesting to note the behaviour of the efficiency as a function of S/N when the seed threshold is lowered slightly to 3.5 (the

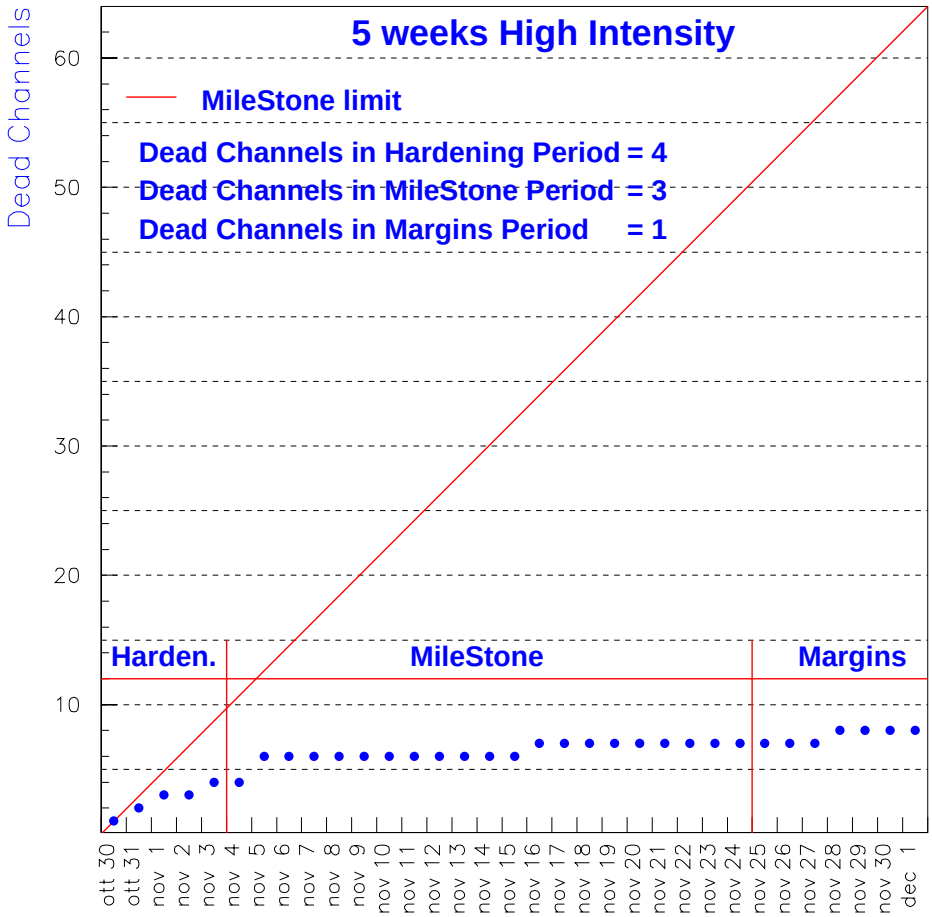

Fig. 20. Summary of all channel losses during the complete high intensity running period.

reader is again referred to the lower plot in Fig. 24). The fall-off of efficiency with S/N is considerably less steep than for the seed threshold of 4, and the efficiency is still in excess of 95 % even for a S/N value as low as 10.
In the above analysis, an important parameter was the size of the window in which hits were searched for around the track. A plot of efficiency as a function of the window size (Fig. 25) shows that the efficiency quickly arrives at a plateau for window width just in excess of the range of the track residuals (see lower plot, Fig. 25). The standard deviation of this distribution *does not* reflect the intrinsic resolution of the detector but rather the degree of multiple scattering prior to that particular chamber. The existence of a plateau confirms the absence of fake noise hits. The size of the window finally chosen for the efficiency studies was 0.4 cm.

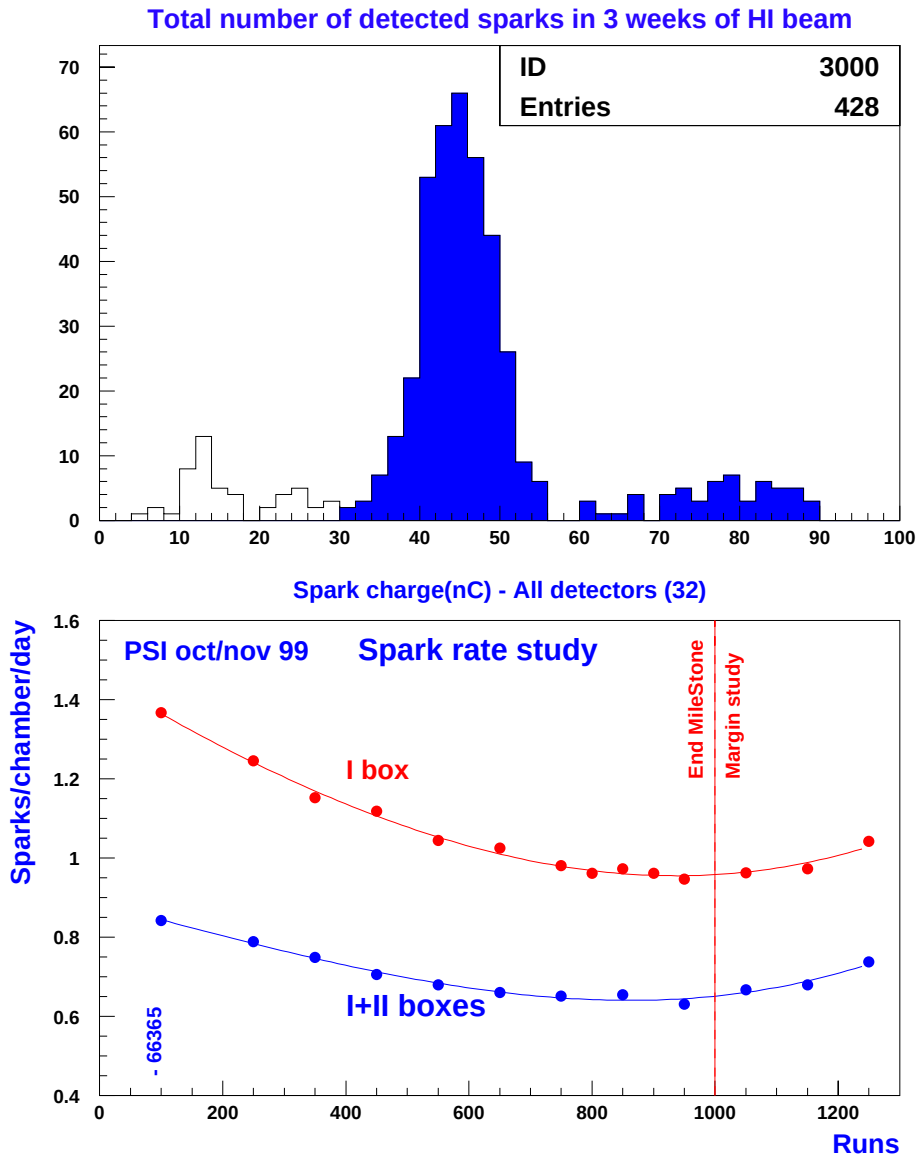

Fig. 21. Distribution of charge within current events identified as sparks (upper plot); average spark rate as a function of run number (lower plot).

4.8 2-D reconstruction capabilities

Four of the detectors in each box were mounted such that their strips were at a small stereo angle ($\tan(\alpha)$=0.1) to those of the other chambers (whose strips were oriented vertically). Two of these stereo chambers were used in conjunction with three normally mounted detectors to investigate 2-D reconstruction capabilities, see Fig. 26. A pattern of holes (ϕ=2 mm) was drilled into a 2 cm thick brass plate which was placed just in front of the first detector crate. Data was recorded for several hours, triggering on the coincidence of the LIF and LIB scintillators with the beam at low intensity (300 Hz/mm^2).
Fig. 27 shows the form of the brass mask and the corresponding images ex-

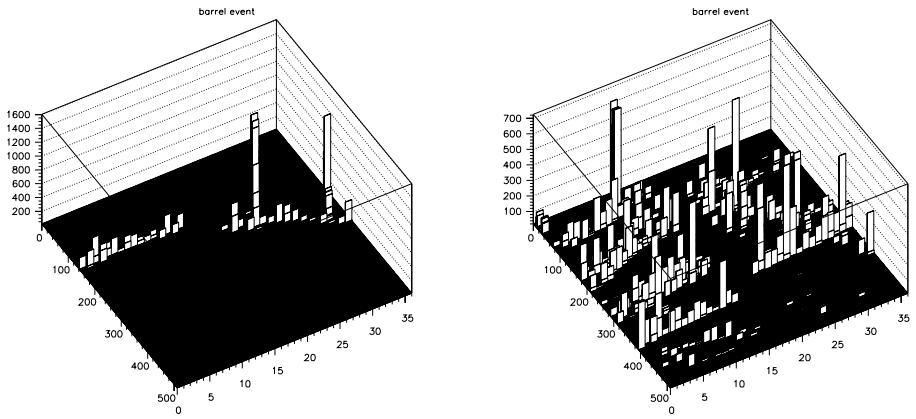

Fig. 22. 'Lego' plots of the pedestal subtracted raw data for all 32 chambers at low intensity (left) and high intensity (right). The region without data in the centre of the plots corresponds to the space occupied by the 'Forward' detectors.

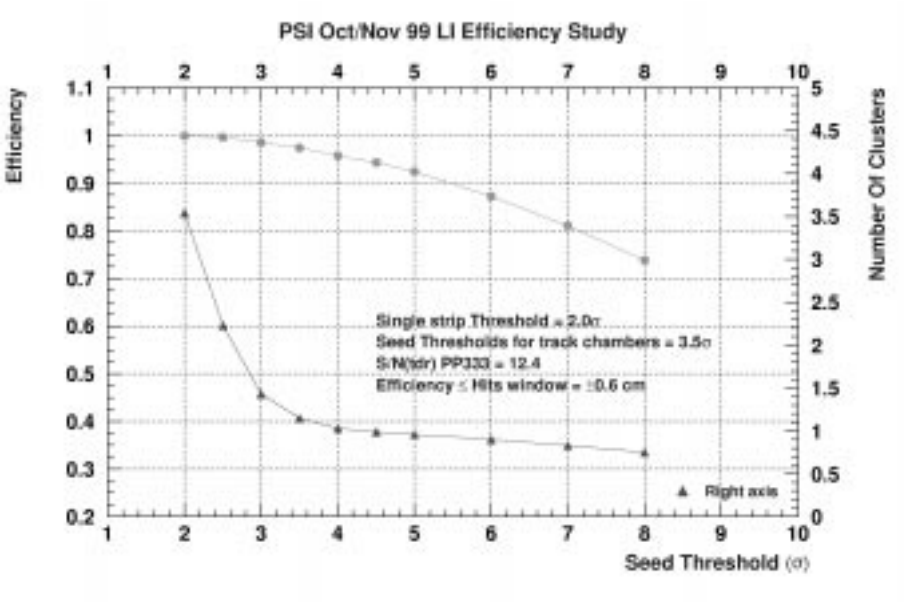

Fig. 23. Efficiency and average number of clusters as a function of seed threshold, for a typical MSGC at the PSI test.

tracted from the data. Simple tracking algorithms were used to reconstruct the points at which the tracks passed through the plane of the mask [3] . A clear image can be discerned even when the raw data is plotted with no cuts. However it was found that the results were cleaner when cuts were applied to the track slope; tracks not passing directly through the holes but instead being scattered into the imaging detectors after interaction with the brass are then

[3] The X coordinates were obtained directly from the hit positions in the vertical chambers; the Y coordinates were calculated using the relation Y = (X_{st}/cos(α) - X)/tan(α), where α is the stereo angle, X_{st} is the hit position in the stereo chamber and X is the hit position in the vertical detectors projected into the plane of the stereo chamber.

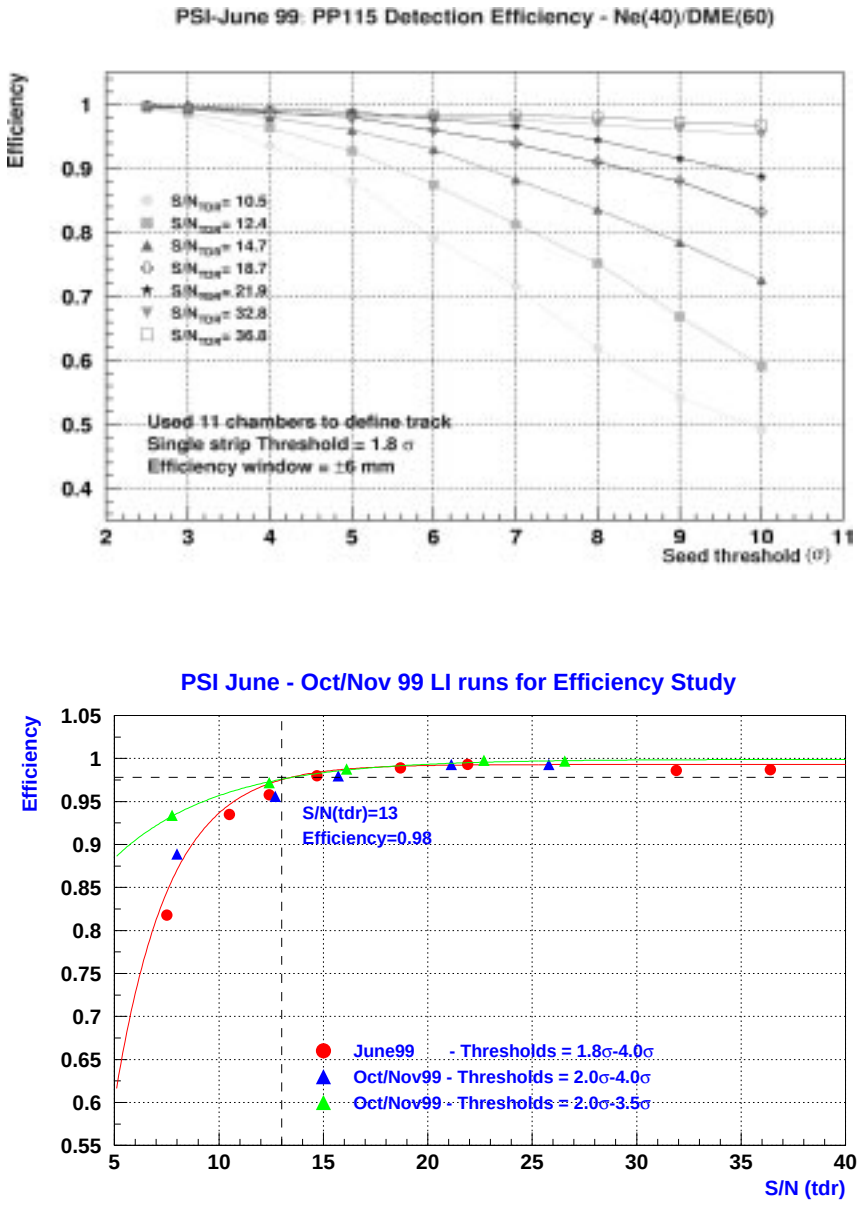

Fig. 24. Efficiency as a function of seed threshold for various S/N values (upper plot) and as a function of S/N with the seed threshold values at 3.5 and 4.0 (lower plot).

largely eliminated. The remaining background after making the cut on the track slope was found to be Gaussian; direct subtraction of this distribution further improved the image contrast.

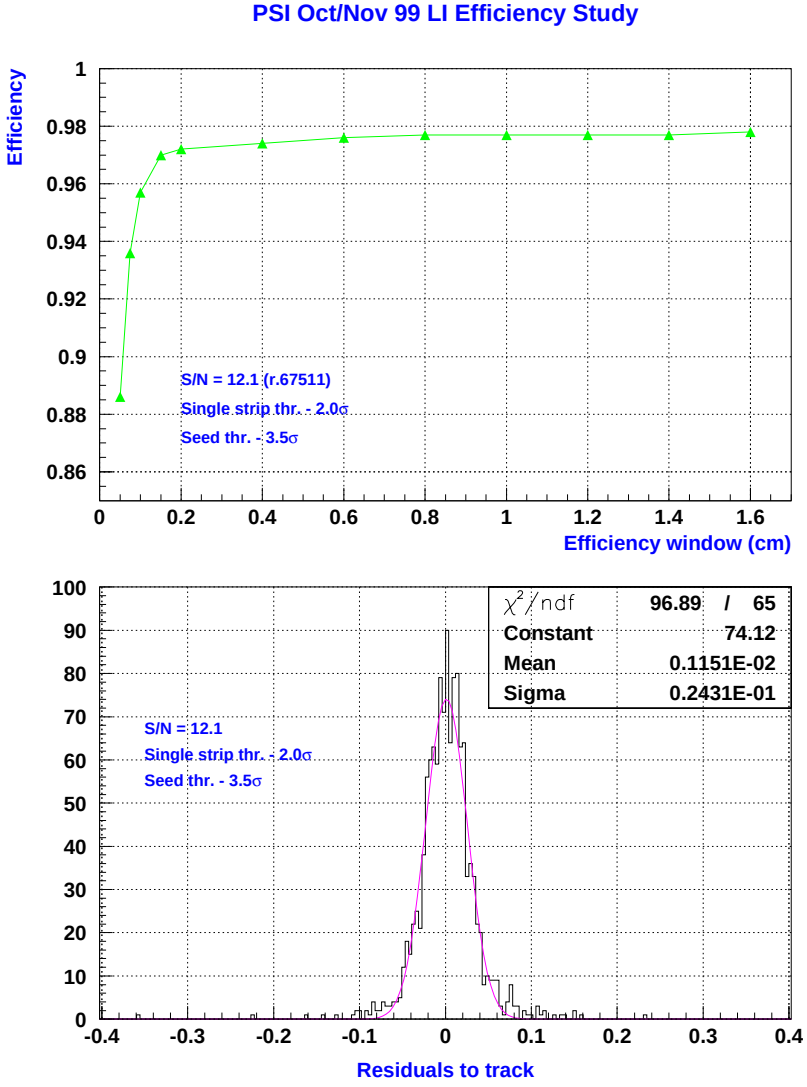

Fig. 25. Efficiency as a function of the size of the window opened around the track (upper plot). The lower plot shows the residuals distribution for one of the chambers.

5 Conclusions

The inner tracking detectors for experiments at future hadron colliders, such as CERN's LHC project, will be subjected to unprecedented radiation fluxes. The spatial resolution and speed requirements for these detectors are also very demanding. We have refined micro-strip gas chamber technology to a level which allows these requirements to be met, while maintaining stable detector operation at high particle rates over long time periods. Convincing evidence to support this statement has been provided by the results of a recent test beam experiment at PSI; these results are summarised below. Assembly, testing and quality control procedures were established, in collaboration with industrial

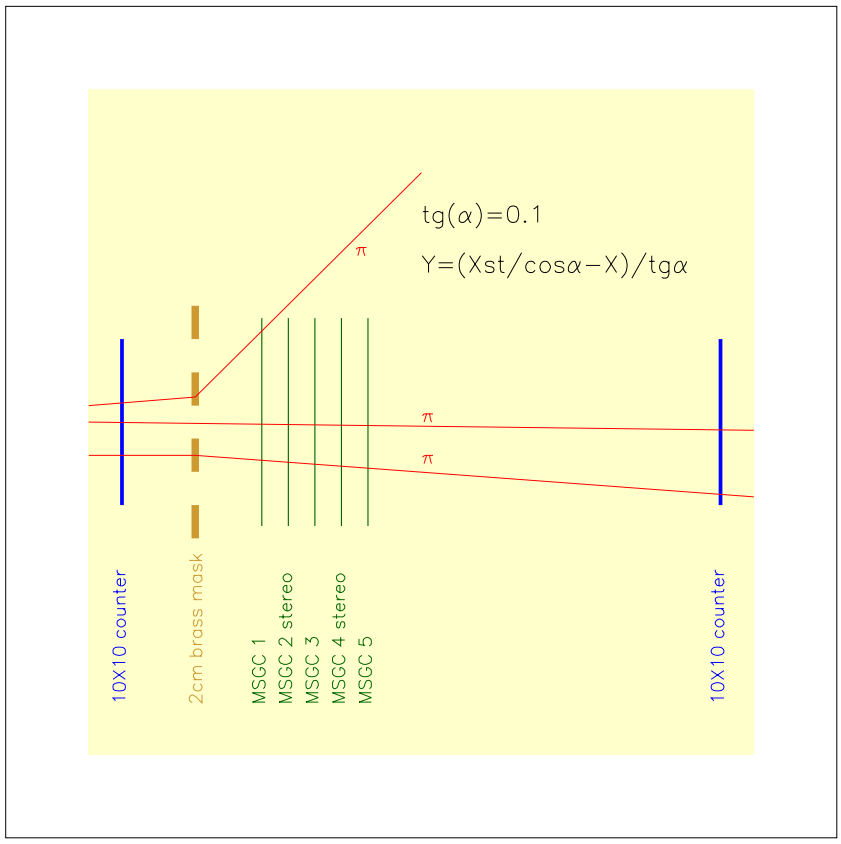

Fig. 26. Layout for the 2-D imaging study.

partners, to allow devices of the required standard to be mass produced.
The beam test was conducted at the PSI πM-1 facility in October/November 1999 and was a Milestone for the LHC Compact Muon Solenoid (CMS) experiment. Thirty-two chambers were installed at PSI and subjected to a high intensity (approximately 6 kHz/mm^2) 350 MeV pion beam, covering the whole active area of the detectors, for a total integrated time of 493 hours. The chambers were operated at an average signal-to-noise ratio of 31; the average cathode voltage was then 515 V, somewhat higher than should be needed to provide 98 % efficiency at CMS using APV electronics. The S/N for all chambers remained constant throughout the whole test period, with no indications of ageing or other gain instabilities.
Each of the 32 chambers had 512 strips, giving an overall total of 16384 channels. Of these, 201 (1.2 %) were defective prior to the high intensity run period (161 lithographic defects, 33 damaged during laboratory testing, 7 lost during transport/installation at PSI). During the 5-week high intensity period, a total of 8 additional dead strips or electronics channels were detected: 4 from the preliminary 'hardening' phase, 3 during the official milestone period and 1 when the voltage margins of the detectors were investigated. The 3 strips lost from 32 chambers in the milestone phase is clearly well within the CMS requirement of 30 dead strips from 25 chambers. The spark rate of the detectors was continuously monitored and was always very low, decreasing to an

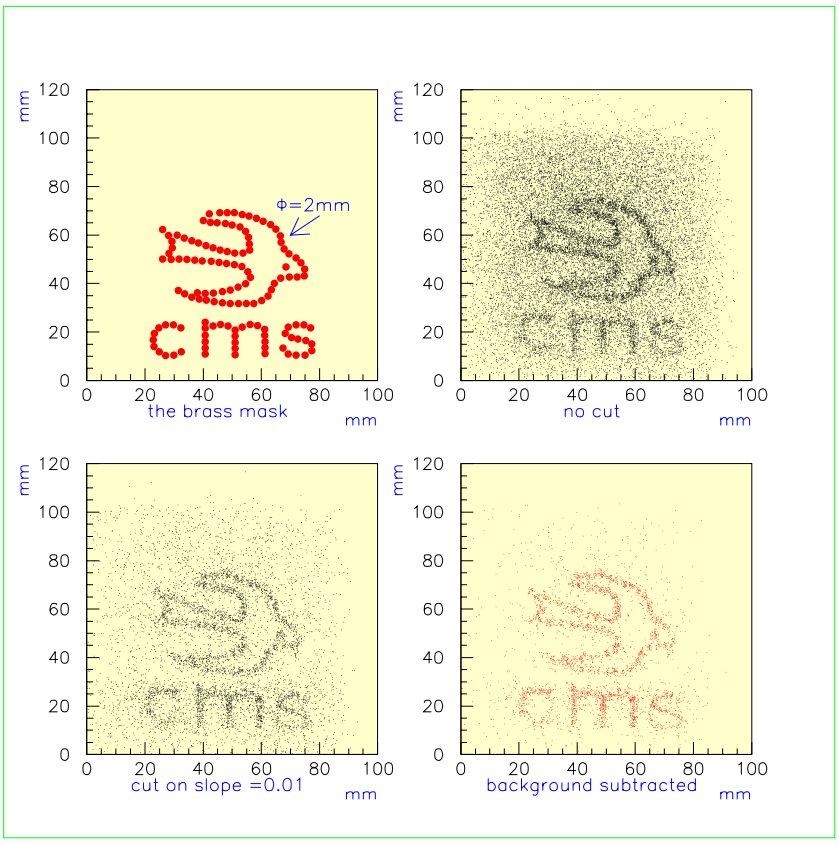

Fig. 27. The pattern of holes in the brass mask used for imaging studies was a swallow and the letters 'CMS'. The image reconstructed from the raw data is shown together with the improved image after application of a cut on the track angle and subtraction of the Gaussian background.

average of less than 1 spark per chamber per day at the end of the test period. One week of high intensity running was devoted to a study of the voltage margins. The cathode voltages of 24 chambers were raised above the normal working point (98 % efficiency at CMS) values. The maximum S/N attained was 2.4 times the usual operating value. During this study, the average spark rate of the detectors increased only very slightly and no unusual degradation of the gain was observed. No increase in the strip loss rate was detected. We conclude that there is considerable scope for increasing the detector voltages should this be necessary (for example to maintain efficiency in the event of unforeseen effects such as higher than expected noise or long-term ageing phenomena).

The signal-to-noise ratio at which 98 % efficiency is achieved was found to be 13, using a threshold of 4.0 sigma. To make fair comparisons (since Premux, not APV, electronics were used at PSI), the chambers were tested at a S/N always in excess of 28. An efficiency of higher than 95 % could still be obtained at S/N $\approx$ 10 using a seed threshold of 3.5 sigma.

A 2 cm thick brass mask was placed in the beam to evaluate the 2-D reconstruction capabilities of the system, using two chambers with strips oriented

at a small stereo angle to the vertical to provide the second coordinate. The pattern of narrow holes in the mask was found to be well resolved.
The excellent MSGC performance during the PSI Milestone test was achieved by careful choice of detector design. The selection of a coated substrate with the highest possible surface resistivity consistent with the required rate capability minimised the risk of sparks between electrodes. This risk was further reduced by sophisticated electrode passivation, use of a 'UV-free' gas mixture and thin anode strips which provided high gain for the minimum possible bias voltage. When sparks did occur, their impact was minimised by the fact that the cathodes were divided into groups of 16, thereby dividing the capacitance and reducing the energy available to the discharge. Lithographic quality and the observance of clean assembly procedures were also important factors. Previous tests at PSI, using substrates with a higher percentage of lithographic defects, yielded somewhat poorer results; in particular, a significantly higher number of strips were lost due to 'hardening' within the first few days of high intensity running. Unexpected shorts between anode and cathode, experienced in previous trials, were completely absent during the Milestone tests. This improvement was achieved following the introduction of tighter cleanliness regulations, both in-house and at the sites of our industrial partners. The avoidance of carbon fibre as a drift window material is also recommended for shorts to be eliminated.

Acknowledgements

We would like to thank the physicists and engineers of the IPN-Lyon HEP group for providing a sophisticated and reliable data acquisition system without which this work would not have been possible. The help and assistance of the PSI liaison staff and in particular of Dr. Dieter Renker is gratefully acknowledged. We would also like to thank Mr. L. Corucci of the INFN mechanics workshop for his skilled technical support.

References

[1] A Oed, **Position-sensitive detector with micro-strip anode for electron multiplication with gases**, Nucl. Instr. and Meth. A263 (1988) 351.

[2] F Angelini, *et al*, **A microstrip gas avalanche chamber with two dimensional read-out**, Nucl. Instr. and Meth. A283 (1989) 755.

[3] F Angelini, *et al*, **The micro-strip gas chamber**, Nucl. Physics 23 A (1991) 254.

[4] R Bouclier, *et al*, **High flux operation of micro-strip gas chambers on glass and plastic supports**, Nucl. Instr. and Meth. A323 (1992) 240.

[5] G Charpak, *et al*, Nucl. Instr. and Meth. 62, 235 (1968).

[6] T Hott, *for the Hera-B Inner Tracker Collaboration*, **MSGC development for the inner tracker of Hera-B**, presented at the 5th International Workshop on B-Physics at Hadron Machines, Los Angeles, 1997, published in Nucl. Instr. and Meth. A408 (1998) 258.

[7] CMS Technical Design Report, CERN/LHCC 98-6.

[8] F Angelini, *et al*, **Microstrip gas chamber with true two-dimensional and pixel read-out**, Nucl. Instr. and Meth. A323 (1992) 229.

[9] R Bellazzini, *et al*, **Electric field, avalanche growth and signal development in micro-strip gas chambers and micro-gap chambers**, La Rivista del Nuovo Cimento, Vol. 17, No. 12 (1994).

[10] F Angelini, *et al*, **Development of a very large area MicroStrip Gas Chamber for the CMS central tracking system**, Nucl. Instr. and Meth. A360 (1995) 22.

[11] J E Bateman, *et al*, **Rate and lifetime characteristics of a gas microstrip detector fabricated on thin D263 glass**, RAL-95-038.

[12] R Bouclier, *et al*, CERN-PPE/92-53 (1992).

[13] N Lumb, **Lifetime characteristics of micro-strip gas chambers**, PhD Thesis, University of Manchester (1996) 84-87.

[14] R Bouclier, *et al*, **Performance of gas microstrip chambers on glass substrates with electronic conductivity**, Nucl. Instr. and Meth. A332 (1993) 100.

[15] F Angelini, *et al*, **Operation of MSGCs with gold strips built on surface treated thin glasses**, Nucl. Instr. and Meth. A382 (1996) 461.

[16] W G Gong, *et al*, **MSGCs with Pestov glass coatings**, Nucl. Instr. and Meth. A374 (1996) 144.

[17] J E Bateman, *et al*, **The experimental characterisation of gas microstrip detectors III: lifetime characteristics**, RAL-94-114.

[18] R Bouclier, *et al*, **Development of micro-strip gas chambers for high rate operation**, Nucl. Instr. and Meth. A367 (1995) 168.

[19] J E Bateman, *et al*, RAL-TR-95-032.

[20] R Bellazzini, *et al*, **Technique for the characterization of discharges in micro-strip gas chambers**, Nucl. Instr. and Meth. A398 (1997) 426.

[21] R Bellazzini, *et al*, **A UV light photo-detector based on a micro-gap chamber with single electron response**, Nucl. Instr. and Meth. A371 (1996) 358.

[22] O. Bouhali, *et al*, **Operation of microstrip gas counters with Ne-DME gas mixtures**, Nucl. Instr. and Meth. A378 (1996) 432.

[23] D Abbaneo, *et al*, **Test of a CMS MSGC Tracker Prototype in a High Intensity Hadron Beam**, Nucl. Instr. and Meth. A409 (1998) 37.

[24] M Huhtinen, **Factors to scale highly ionising particle rates in MSGC irradiation tests to the LHC radiation environment.**, CMS Note 1997/073.

[25] L L Jones, **Premux 128 specification, version 2.1** (1994).

[26] G Claus, *et al*, **Strip detectors read-out system user's guide**, CRN Strasbourg report CRN 96-33 (1996).

[27] M Morrissey, Imperial College, London (1996).

[28] Creative Electronics Systems, Route du Pont-Butin 70, CH-1213 Petit-Lancy, 1/Geneva, Switzerland.

[29] R Malina, *et al*, **High rate tests of micro-strip gas chambers for CMS**, Nucl. Physics B (Proc. Suppl.) 78 (1999) 80.

[30] F G Sciacca, *et al*, **Readout of micro strip gas chambers for the CMS central tracker with the APV6 front-end chip**, CMS Conference Report, CMS CR 1998/018.